Replicative history marks transcriptional and functional disparity in the CD8+ T cell memory pool

Bresser, K.; Kok, L.; Swain, A.C.; King, L.A.; Jacobs, L.; Weber, T.S.; ... ; Schumacher, T.N.

nature immunology

ARTICLES

https://doi.org/10.1038/s41590-022-01171-9

Replicative history marks transcriptional and functional disparity in the CD8+ T cell memory pool

Kaspar Bresser[1,10], Lianne Kok[1,10], Arpit C. Swain[2], Lisa A. King[1,9], Laura Jacobs[1], Tom S. Weber[3,4], Leïla Perié[5], Ken R. Duffy[6], Rob J. de Boer[2], Ferenc A. Scheeren[7] ✉ and Ton N. Schumacher[1,8] ✉

Clonal expansion is a core aspect of T cell immunity. However, little is known with respect to the relationship between replicative history and the formation of distinct CD8+ memory T cell subgroups. To address this issue, we developed a genetic-tracing approach, termed the DivisionRecorder, that reports the extent of past proliferation of cell pools in vivo. Using this system to genetically 'record' the replicative history of different CD8+ T cell populations throughout a pathogen-specific immune response, we demonstrate that the central memory T (T_{CM}) cell pool is marked by a higher number of prior divisions than the effector memory T cell pool, owing to the combination of strong proliferative activity during the acute immune response and selective proliferative activity after pathogen clearance. Furthermore, by combining DivisionRecorder analysis with single-cell transcriptomics and functional experiments, we show that replicative history identifies distinct cell pools within the T_{CM} compartment. Specifically, we demonstrate that lowly divided T_{CM} cells display enriched expression of stem-cell-associated genes, exist in a relatively quiescent state, and are superior in eliciting a proliferative recall response upon activation. These data provide the first evidence that a stem-cell-like memory T cell pool that reconstitutes the CD8+ T cell effector pool upon reinfection is marked by prior quiescence.

The CD8+ T cell compartment serves to provide protection against intracellular pathogens and also acts as a modifier of cancer growth. Upon antigen encounter, naive T (T_N) cells undergo extensive gene-expression alterations while entering a highly proliferative state, dividing every 4 to 6 hours[1,2] in mice. This phase of clonal expansion gives rise to a phenotypically and functionally diverse pool of effector T cells (T_{EFF}) that exceeds its precursor population size by >10,000-fold[3,4]. Unlike T_N cells, these T_{EFF} cells have the capacity to disseminate to peripheral tissues, and can scan for and kill infected or transformed cells. Upon antigen clearance, around 95% of the T_{EFF} pool succumbs to apoptosis, leaving behind a small long-lived pool of memory T (T_M) cells that is equipped to provide long-term protection against recurring pathogens.

The central role of proliferation in the T cell response has inspired many to study the relationship between replication and T cell state. While earlier work hinted that memory precursor T cells have undergone limited clonal expansion[5,6], more recent work studying acute T cell responses in humans demonstrated that T_M cells, as a whole, are derived from precursor cells that have undergone an extensive number of divisions[7]. Furthermore, prior work has shown that cell cycle speed can differ substantially between phenotypically distinct T cell subsets at different time points in the T cell response. Specifically, T_{CM} cells, a subgroup of memory cells that are endowed with a high level of multipotency, have been documented to undergo homeostatic proliferation after pathogen clearance, while effector memory T (T_{EM}) cells have a low turnover rate[8,9]. In contrast, during the effector phase, a T_{CM}-like state has been linked to lower division speed and reduced clonal burst size compared with that of their T_{EM}-like and terminally differentiated counterparts[10–13].

The phase-dependent association of proliferative activity within specific cell states, in combination with the reported phenotypic instability of certain T cell subsets[14,15], makes it difficult to deduce the replicative history (that is, the cumulative number of prior divisions) of different T_M cell populations and the possible relationship between replicative history and functional properties. Here, we develop a genetic-tracing approach—termed DivisionRecorder—that allows for the measurement of prior division of cell pools over extensive rounds of division, and we apply this approach to determine to what extent replicative history identifies distinct T_M cell states and behaviors. In this effort, we focus on three central issues: (1) what are the differences in replicative history between (precursor-)T_{CM} and T_{EM} cells in the effector and memory phase? (2) Is there heterogeneity in prior division within the T_{CM} pool? (3) If so, does replicative history of cells within the T_{CM} pool predict their capacity to mount a secondary T cell response?

Results

Division-linked genetic labeling of cell pools. The genome contains a large number of hypervariable short tandem nucleotide repeats (STRs) that accumulate intra-allelic length mutations

[1]Division of Molecular Oncology & Immunology, Oncode Institute, The Netherlands Cancer Institute, Amsterdam, the Netherlands. [2]Theoretical Biology and Bioinformatics, Utrecht University, Utrecht, the Netherlands. [3]The Walter and Eliza Hall Institute of Medical Research, Melbourne, Victoria, Australia. [4]The Department of Medical Biology, The University of Melbourne, Melbourne, Victoria, Australia. [5]Institut Curie, Université PSL, Sorbonne Université, CNRS UMR168, Laboratoire Physico Chimie Curie, Paris, France. [6]Hamilton Institute, Maynooth University, Maynooth, Ireland. [7]Department of Dermatology, Leiden University Medical Center, Leiden, the Netherlands. [8]Department of Hematology, Leiden University Medical Center, Leiden, the Netherlands. [9]Present address: Department of Medical Oncology, Amsterdam UMC, Vrije Universiteit Amsterdam, Cancer Center Amsterdam, Amsterdam, the Netherlands. [10]These authors contributed equally: Kaspar Bresser, Lianne Kok. ✉e-mail: f.a.scheeren@lumc.nl; t.schumacher@nki.nl

through DNA polymerase slippage during cell division. Such slippage mutations in endogenous STRs have been used to study lineage trees in various organisms and tissues[16,17], and synthetic STRs have previously been employed in a probabilistic-labeling approach to define stem cells in the intestinal epithelium and the mammary gland[18,19]. To investigate the replicative history of T_M cells, we engineered a synthetic STR-reporter system to continuously 'record' proliferation in cell pools. This genetically encoded system, termed DivisionRecorder, utilizes a synthetic STR domain to achieve a division-linked low-probability acquisition of a fluorescent mark (Fig. 1a). The DivisionRecorder consists of two separate elements: (1) a retroviral-vector encoded module that contains a synthetic STR linked to an out-of-frame CRE recombinase gene; and (2) a CRE-activity reporter module that irreversibly induces the expression of a red fluorescent protein (RFP). In its base configuration, all cells that contain the DivisionRecorder express only GFP (hereafter referred to as DR^{GFP} cells). As cells undergo successive divisions, slippage mutations that occur within the synthetic STR yield in-frame variants of the downstream CRE recombinase gene at a fixed, division-dependent, probability (p). The resulting CRE activity induces an irreversible activation of the RFP gene, giving rise to GFP^+RFP^+ cells (hereafter referred to as DR^{RFP}) that pass this genetically encoded label on to subsequent generations, resulting in a cumulative increase in the DR^{RFP} cell fraction within the DivisionRecorder$^+$ (DR^+, that is, the sum of DR^{GFP} and DR^{RFP}) population as the cell pool expands (Fig. 1b and Supplementary Note 1). Importantly, when p is small (< 0.01) the DivisionRecorder yields a near-linear relationship between the DR^{RFP} fraction and the average number of divisions over dozens of population doublings (Fig. 1c)[20], thereby allowing analysis of replicative history—at the population level—far beyond what can be achieved with classical cell-labeling dyes[21] (Fig. 1d).

To test the utility of the DivisionRecorder, we established a reporter cell line carrying a lox-STOP-lox-RFP cassette. Following retroviral introduction of the GFP-STR-CRE module, a progressive increase in DR^{RFP} cells was observed over time, whereas no label acquisition was observed when the STR was replaced with a stable DNA sequence (Fig. 1e,f). Moreover, the rate at which DR^{RFP} cells accumulated was dependent on the sequence stability of the STR[22,23], underpinning that p is linked to the likelihood of STR slippage (Fig. 1g). Similarly, upon introduction of the DivisionRecorder into immortalized embryonic fibroblasts from the Ai9 mouse strain—which carries an endogenous lox-STOP-lox-RFP cassette[24]—a low and predictable DR^{RFP} cell acquisition was observed, with a [G]33 STR conferring a p of 0.0052 ± 0.00074 (Fig. 1h,i), thereby enabling the measurement of replicative history over many cell divisions (in theory >1,500 population doublings, Fig. 1d).

To test whether the DivisionRecorder can be used as a proxy for replicative history in the $CD8^+$ T cell compartment in vivo, we generated Ai9;OT-I mice, in which all T cells recognize the $OVA_{257–264}$ epitope, thereby allowing examination of T cell pools in the context of equal TCR affinity. Ai9;OT-I T cells were isolated, modified with the DivisionRecorder to obtain DR^+ OT-I T cells and transferred into *Listeria monocytogenes*-OVA (*Lm*-OVA) infected mice, and the fraction of DR^{RFP} cells was measured over time (Fig. 2a). At early time points following cell transfer (d1–d4), a rapid increase in DR^{RFP} cells was observed (Fig. 2b,c), coinciding with the proliferative burst of the antigen-specific $CD8^+$ T cell pool. To determine whether the observed accumulation of DR^{RFP} cells formed an accurate measure of prior cell division, DR^+ OT-I T cells were stained with CellTrace Violet (CTV) prior to cell transfer. Notably, analysis of the fraction of DR^{RFP} cells within cell pools with different degrees of CTV dilution revealed a close correlation (Fig. 2d,e, $r_{rm} = 0.94$), providing direct evidence that in vivo DR^{RFP} acquisition reflects the extent of past division in the $CD8^+$ T cell pool. In conclusion, these data establish that the DivisionRecorder allows for long-term measurement of division history in cell pools in vivo, in a way that is compatible with downstream methodologies such as single-cell sequencing (see below).

$CD8^+$ T_{CM} cells are derived from replicative mature T cells. Having validated the utility of the DivisionRecorder to record T cell division, we next sought to determine the replicative history of the total $CD8^+$ T_M pool relative to that of the T_{EFF} pool. Analysis of the size of the DR^+ OT-I T cell compartment in blood following *Lm*-OVA infection showed the characteristic rapid expansion phase, with T cell numbers peaking around day 6, and subsequent contraction into a stable memory pool (Fig. 3a). Notably, DR^{RFP} cells remained detectable following formation of T cell memory, thus allowing analysis of replicative history at late time points after infection (Fig. 3b).

If T_M cells are primarily derived from T cells that underwent limited proliferation upon first encounter of the antigen, the fraction of DR^{RFP} cells would be expected to decay during the contraction phase, owing to the decline in the number of clonally expanded T_{EFF} cells (Extended Data Fig. 1 and Supplementary Note 3). However, analysis of DR^{RFP} frequencies in blood demonstrated that the fraction of DR^{RFP} cells did not decline, but instead continued to increase during the contraction and memory phase (an increase of $2.07\% \pm 0.77\%$ between day 13 and 59, Fig. 3c). This increase in DR^{RFP} frequencies following pathogen clearance was not restricted to T cell responses induced by *Lm*-OVA infection, but was also observed upon infection with LCMV-OVA[25] (Fig. 3d), and was not due to anatomical redistribution of cells with distinct division histories, as the fraction of DR^{RFP} cells increased concurrently in peripheral blood and the primary sites of *Lm*-OVA infection (spleen/liver; Fig. 3e,f). Thus, in line with work by Akondy et al.[7], our results support the notion of a replicative 'mature', rather than 'nascent', $CD8^+$ T_M pool, and extend this observation beyond the peripheral blood compartment to the sites of infection.

It has been well documented that T_{CM} cells are able to maintain the memory pool through infrequent homeostatic cell division[15,26,27], and recent work has shown that precursor-T_{CM} cells slow down their replicative cycle early in the expansion phase[10], suggesting limited clonal expansion of these cells during the early phase of the T cell response. However, it is difficult to translate cell cycle activity at a given time point into cumulative proliferative history, and we therefore wished to directly test the relationship between cell state (for example, T_{CM} or T_{EM}) and replicative history during different stages of the T cell response. To this end, the fraction of DR^{RFP} cells within the T_M pool was calculated at varying expression levels of proteins associated with either multipotency or terminal differentiation (Fig. 3g). This analysis revealed a positive correlation between replicative history and the expression of the T_{CM}-associated proteins CD27 ($r_{rm} = 0.81$, $P = 6.2 \times 10^{-14}$) and CD62L ($r_{rm} = 0.62$, $P = 5.6 \times 10^{-7}$)[15,28,29], and a negative relationship between prior division and the expression of the T_{EM}-associated proteins KLRG1 ($r_{rm} = -0.83$, $P = 9.0 \times 10^{-15}$) and CX_3CR1 ($r_{rm} = -0.75$, $P = 4.5 \times 10^{-11}$)[14,15,30]. Likewise, defining multipotent T_{CM} and terminally differentiated T_{EM} subsets by joint expression or absence of CD62L and CD27, respectively, (Extended Data Fig. 2a) and further partitioning on the basis of the expression of KLRG1 or CX_3CR1 revealed a positive association between division history and a less differentiated cell state (Extended Data Fig. 2b). Furthermore, the division history of $CD27^{hi}KLRG1^{lo}$ T_{CM} cells present in lymph nodes equaled that of T_{CM} cells in the spleen, implying that division history is dictated by cell state rather than anatomical location (Extended Data Fig. 2c).

Next, to delineate at which point the divergence in replicative history between T cells with a T_{CM}-like multipotent and T_{EM}-like terminally differentiated phenotype developed, we assessed the link between phenotypic marker expression and DR^{RFP} fractions throughout the T cell response. Notably, replicative history varied

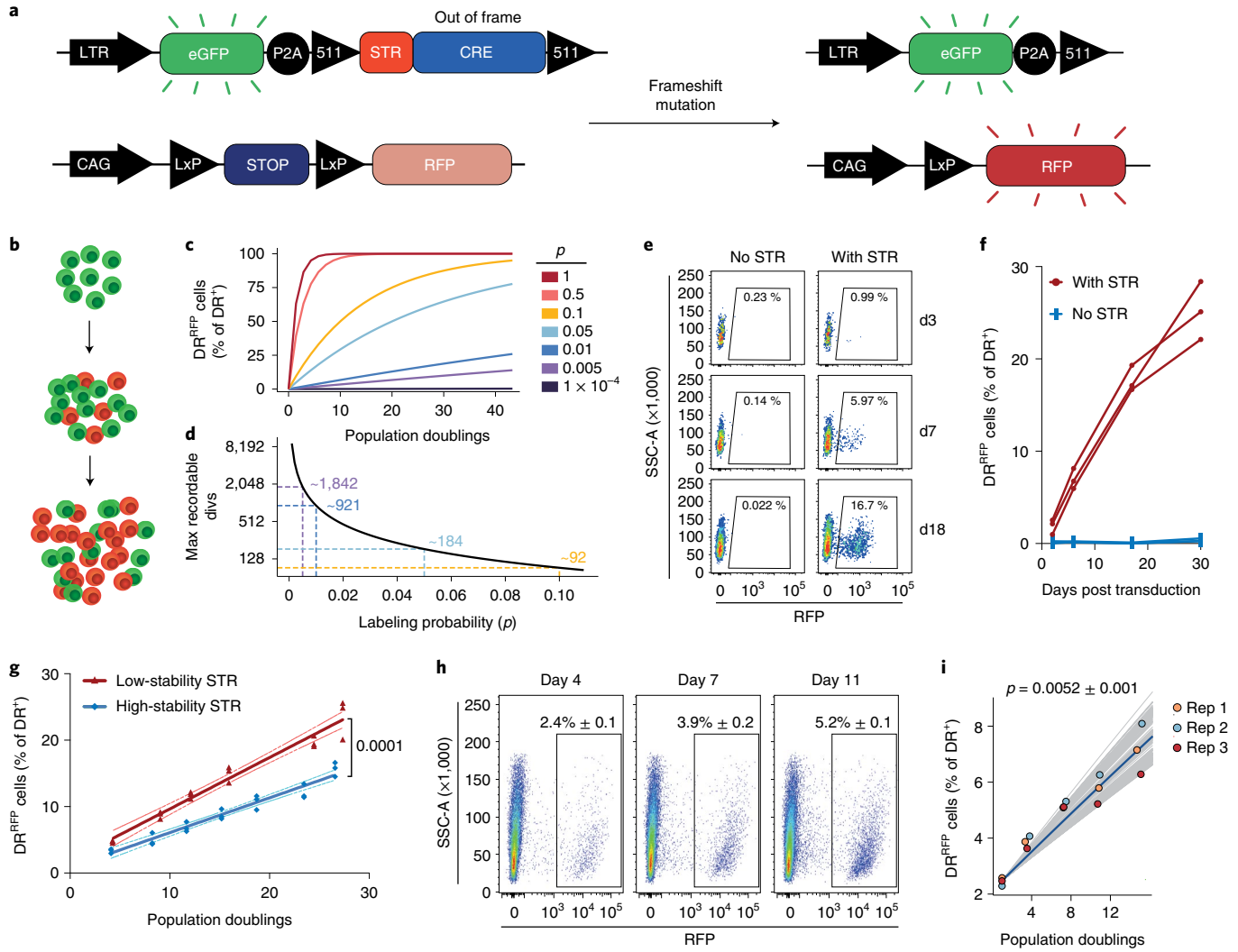

Fig. 1 | DivisionRecorder activation is a proxy for replicative history. a, Schematic overview of the DivisionRecorder system. **b**, Cartoon depicting progressive DivisionRecorder activation in a proliferating cell pool. **c**, Simulation of the minimal ODE model (see Supplementary Note 2 for detailed description and equations), depicting DR^{RFP} acquisition as a function of population doublings for the indicated values of DR^{RFP} acquisition probability (*p*). **d**, Maximal number of theoretically recordable population doublings, approximated by calculating the number of division events required to reach a 99% DR^{RFP} population. Approximate maximums for selected values of *p* are indicated, colors correspond to legend in **c**. **e**,**f**, Percentage of DR^{RFP} cells over time i n cultured DivisionRecorder$^+$ (DR^+) CRE-activity reporter HEK 293T cells ($n = 3$ replicates per group) in which the CRE recombinase gene was preceded by either a stable nucleotide region (indicated as 'no STR') or a repeat of 24 guanines (indicated as 'with STR'). Representative plots (**e**) and summarizing line graphs (**f**) are shown. Lines connect experimental replicates. **g**, Percentage of DR^{RFP} cells across population doublings in DR^+ CRE-activity reporter HEK 293T cells ($n = 3$ replicates per group) in which the CRE recombinase gene was preceded by either a low-stability STR ([G]24) or a high-stability STR ([CA]30). Dots indicate individual samples, lines represent fitted linear regression, dotted lines indicate bounds of the 95% confidence interval. **h**,**i**, Percentage of DR^{RFP} cells across population doublings in immortalized DR^+ mouse embryonic fibroblasts. Representative flow cytometry plots (**h**) and a summary graph (**i**) are shown. Best fits of the minimal ODE model are depicted (100 bootstraps per experimental replicate, Supplementary Note 2). The blue line represents the median of the bootstraps, gray lines represent individual fits, dots indicate experimental measurements ($n = 3$ replicates). *p* indicates the estimated DR^{RFP} acquisition probability. Depicted experimental data are representative of at least two independent experiments. The *P* value in **g** was determined by two-sided analysis of covariance (ANCOVA).

minimally across T_{EFF} cell states at the peak of the antigen-specific T cell response (d6 post transfer, Fig. 3h and Extended Data Fig. 2d–f), followed by selective accumulation of DR^{RFP} within the $CD27^{hi}KLRG1^{lo}$ early-T_{CM} pool directly after the peak of the expansion phase (Fig. 3h,i and Extended Data Fig. 1g), owing to continued replicative activity of this subset (Fig. 3j,k). The observation that the division history of $CD27^{lo}KLRG1^{hi}$ T cells stays constant after the effector phase (Fig. 3i) suggests that, in addition to the previously documented lack of proliferative activity of this cell pool[15,26,31], this terminally differentiated subset does not receive notable replenishment by the replicative active $CD27^{hi}KLRG1^{lo}$ T cell pool (Extended Data Fig. 1h). The substantial number of divisions that we observe in the $CD27^{hi}KLRG1^{lo}$ cell pool at the peak of the response appears at odds with the proposed limited clonal expansion of precursor-T_M cells. However, these observations may either be reconciled by the reported trans-differentiation between T_{EFF} cell states[14,15,30], or by the fact that a reduced proliferative activity may form a property of only a small part of the memory precursor pool[10,11,32]. In summary, the above data indicate that the high amount of prior division of the T_{CM} pool results from both strong

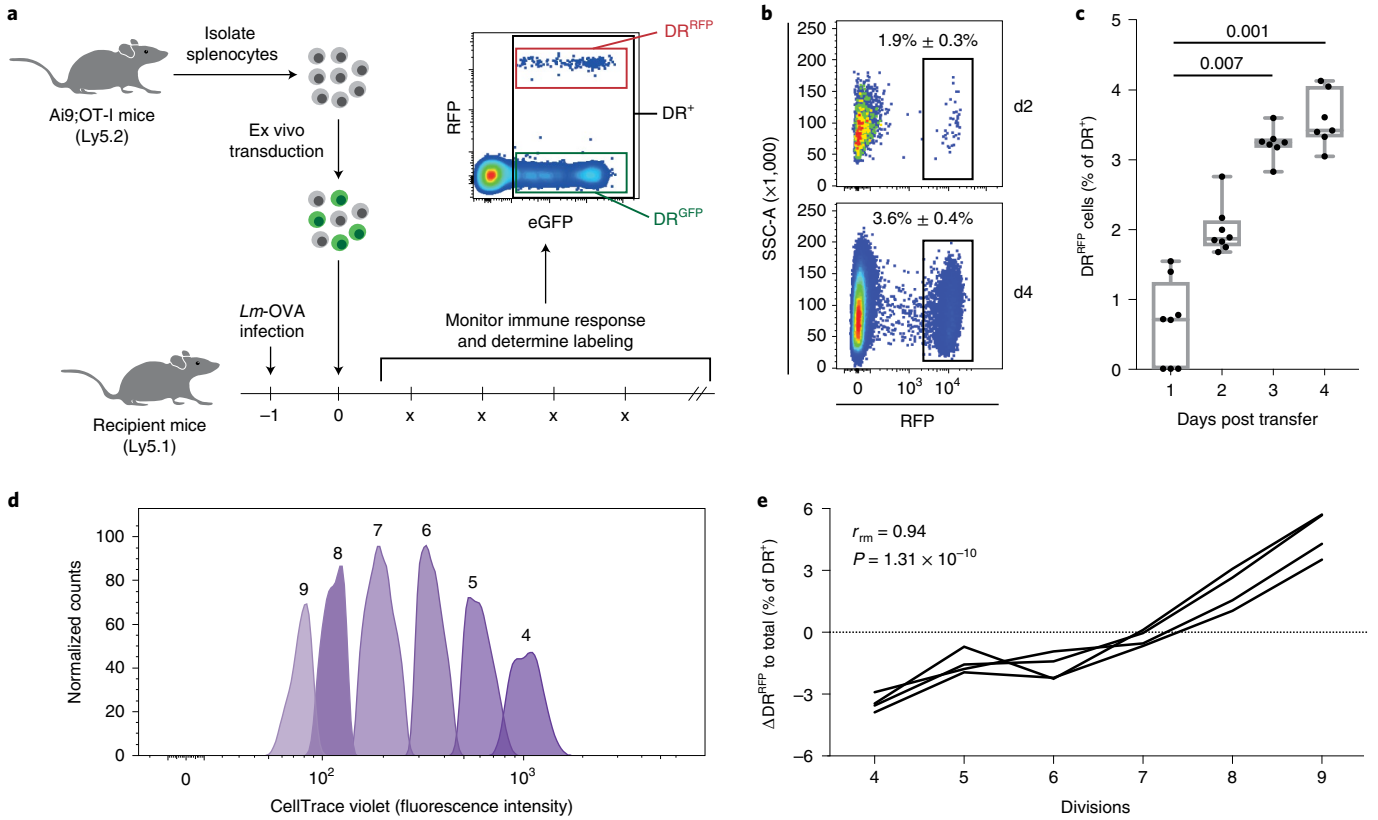

Fig. 2 | The DivisionRecorder can be applied to study T cell division kinetics in vivo. a, Overview of experimental setup. **b**,**c**, DR+ OT-I T cells were transferred into recipient mice 24 hours post infection with *Lm*-OVA. Spleen samples were analyzed for the percentage of DR^{RFP} cells at day 1-4 post cell transfer. Representative pseudo-color density plots (**b**), and boxplots (**c**) in which the boxes indicate group median and 25th/75th percentiles, whiskers represent min/max, dots represent individual samples (n = 8 mice for day 1 and 2; n = 7 mice for day 3 and 4). **d**,**e**, CTV-stained OT-I T cells were retrovirally transduced with the DivisionRecorder and transferred into recipient mice ($n = 4$) 24 hours following infection with *Lm*-OVA. At 48 hours after transfer, splenic DR+ OT-I T cells were assessed for CTV dilution (**d**), and the percentage of DR^{RFP} cells within each division peak was analyzed (**e**). All depicted data are representative of at least two independent experiments; lines and symbols indicate individual mice or samples. *P* values were determined by two-sided Kruskal–Wallis test, with Dunn's multiple-comparisons test (**c**), or two-sided repeated-measurement correlation test (**e**).

proliferative activity during the effector phase and selective proliferative activity after pathogen clearance.

Replicative history identifies distinct T_{CM} cell states. Increasing evidence suggests that the T_{CM} pool is highly heterogeneous in terms of both gene-expression profiles and prior and ongoing replicative behavior[14,15,33], providing an incentive to test for possible associations between division history and transcriptional states within this cell pool. To this end, we carried out single-cell mRNA sequencing (scRNAseq) on DR^{GFP} and DR^{RFP} memory OT-I T cells (75–85 days following *Lm*-OVA infection; Extended Data Fig. 3). In addition, to test whether DR+ OT-I T_M cells assume the same spectrum of transcriptional states as non-modified T cells, we performed scRNAseq on OT-I T_M cells that were generated through adoptive transfer of a small number (2,000) of naive OT-I T cells, followed by *Lm*-OVA infection 24 hours later. DR+ OT-I and unmodified OT-I T_M cells were jointly grouped into 23 transcriptionally distinct MetaCells (MCs)[34], including 4 T_{EM} and 19 T_{CM} MCs, on the basis of the expression of a small set of multipotency- and effector-associated genes (Fig. 4a,b). Notably, while T_M cells derived from small numbers of unmodified OT-I T cells showed a proportionally greater contribution to T_{EM} MCs—consistent with the relationship between precursor frequency and T_{EM} formation[35]—DR+ OT-I T cells and unmodified OT-I T cells were equal in their potential to yield the 19 distinct T_{CM} MCs (Extended Data Fig. 4), indicating that the introduction of the DivisionRecorder did not measurably impact the ability of T cells to differentiate into different T_{CM} states.

Among the observed T_{CM} MCs, two transcriptionally distinct subgroups could be identified (Fig. 4b). Specifically, while all T_{CM} cells showed the expected high expression of *Bcl2*, *Sell*, and *Cd27* and minimal expression of *Cx3cr1*, *Zeb2*, *Gzma*, and *Prdm1* (Fig. 4c and Extended Data Fig. 5a), a dichotomy was observed in the expression of multipotency-associated (for example, *Myb* and *Ccr7*) and effector-associated (for example, *Tbx21* and *Lgals1*) genes within the T_{CM} pool (denoted as T_{CM}(mult.) and T_{CM}(eff.), respectively in the figures; Fig. 4b and Extended Data Fig. 5a). Next, we assessed the relationship between transcriptional state and replicative history within the T_M cell pool. In line with the flow cytometry data, the replicative history of T_{CM}—as a whole—exceeded that of T_{EM}, thereby validating the scRNAseq approach. Strikingly, T_{CM} cells enriched for effector genes had overall higher DR^{RFP}/DR^{GFP} ratios compared with T_{CM} cells enriched for multipotency genes, demonstrating that stemness-related transcriptomic features are inversely associated with division history within the T_{CM} pool (Fig. 4d). Correspondingly, comparison of the three T_{CM} MCs with the highest and lowest level of prior division (hdT_{CM} and ldT_{CM}, respectively) revealed that ldT_{CM} cells were marked by the expression of key multipotency-associated genes, including *Tcf7*, *Sell*, *Myb*, and *Eomes*, and several survival factors (*Gimap* and *Birc* family members, Extended Data Fig. 5b,c). Moreover, one ldT_{CM} MC

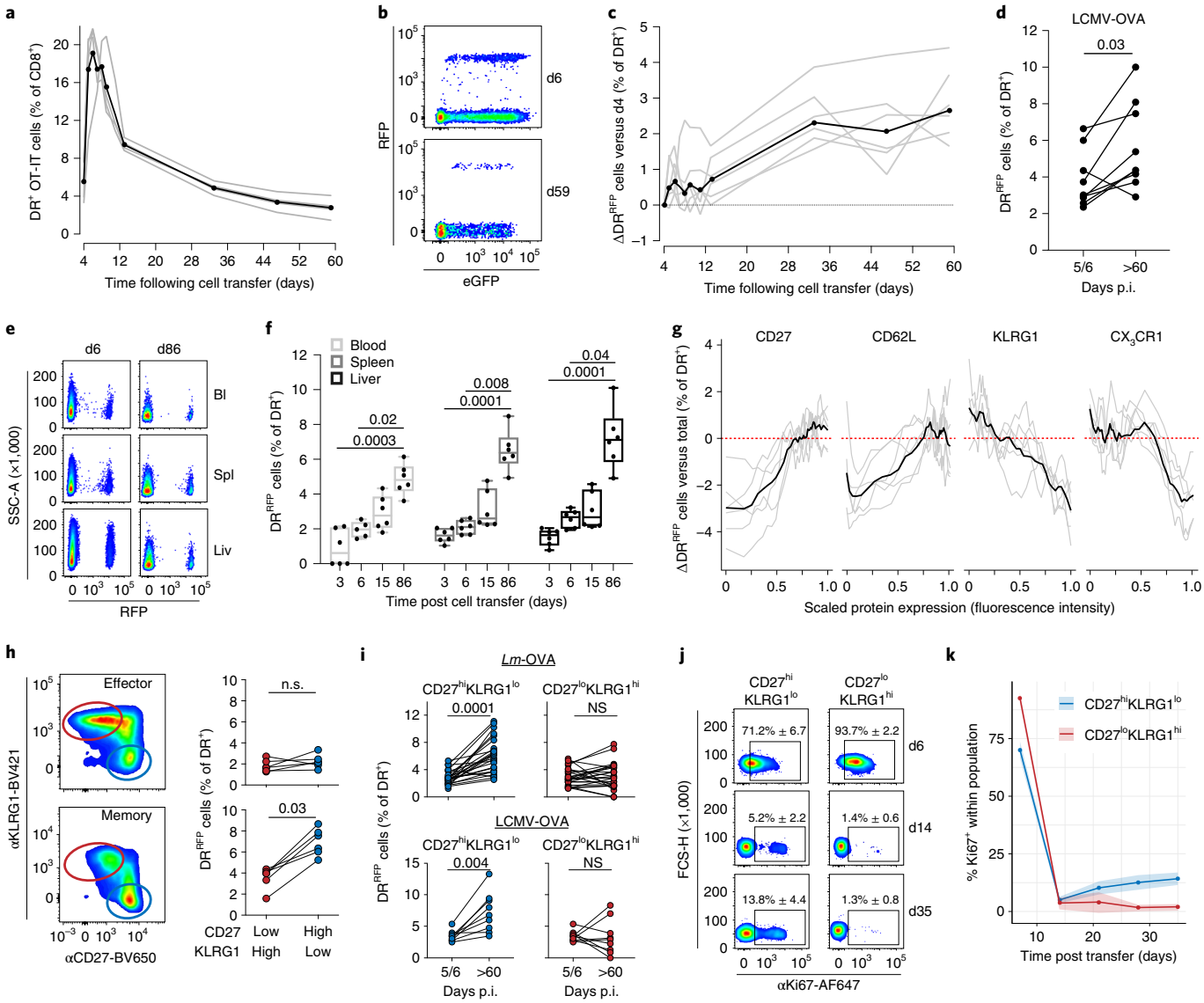

Fig. 3 | The multipotent T_M cell pool is formed by replicative 'mature' cells. a–c, Kinetics of DR+ OT-I T cells (**a**) and the percentage of DR^{RFP} relative to day 4 (**c**) in response to *Lm*-OVA, measured in peripheral blood ($n=6$ mice). Representative flow cytometry plots (**b**) showing DR^{RFP} and DR^{GFP} frequencies at indicated time points, and line graphs (**a**,**c**) depicting kinetics of single mice (gray) and group median (black). **d**, DR^{RFP} percentages within blood at day 5/6 (T_{EFF}) and day >60 (T_M) following LCMV-OVA infection ($n=7$). **e**, Representative plots depicting DR^{RFP} frequencies in blood (Bl), spleen (Spl), and liver (Liv). **f**, Percentage of DR^{RFP} cells detected in the indicated organs of recipient mice at the indicated time points ($n=6$ mice per time point; response to *Lm*-OVA). Boxplots indicate the group median and 25th and 75th percentiles, whiskers represent the minimum and maximum, and dots represent individual samples. **g**, Moving average of surface marker expression level on splenic DR+ cells plotted against the percentage of DR^{RFP} cells within each window during the memory phase (day 86; $n=6$); means are shown in black. DR^{RFP} percentages within each window are corrected for the total percentage of DR^{RFP} cells detected in that sample. **h**, Gating strategy (left) and DR^{RFP} percentages (right) of $CD27^{hi}KLRG1^{lo}$ and $CD27^{lo}KLRG1^{hi}$ cells in spleen during the effector (d6, top) and memory phases (d86, bottom; $n=6$) in response to *Lm*-OVA. **i**, DR^{RFP} percentages within the $CD27^{hi}KLRG1^{lo}$ and $CD27^{lo}KLRG1^{hi}$ cell populations in blood, comparing effector (day 5/6) and memory (day > 60) phases. Data are shown for *Lm*-OVA (top; $n=22$) and LCMV-OVA (bottom; $n=7$) infections. Lines connect data from individual mice. **j**,**k**, Ki67 expression by $CD27^{hi}KLRG1^{lo}$ and $CD27^{lo}KLRG1^{hi}$ OT-I cells in blood in response to *Lm*-OVA. Representative flow cytometry plot (**j**) and line graphs (**k**) in which solid lines indicate population means and shaded areas indicate the 95% confidence interval ($n=11$ mice). All depicted data are representative of at least two independent experiments; lines and symbols indicate individual mice or samples. *P* values were determined by two-sided Kruskal–Wallis test with Dunn's multiple-comparisons test (**f**) or two-sided Wilcoxon's signed-rank test (**d**,**h**,**i**).

was highly enriched for transcripts involved in inhibitory function (*Lag3*, *Cd160*, *Tox*), suggesting a possible analogy with the inhibitory signaling-dependent T_{CM}-precursor subset identified by Johnnidis et al.[33] (Extended Data Fig. 5c). In contrast, hdT_{CM} cells commonly expressed genes related to terminal differentiation, such as *Lgals1* and *S100* family members, and showed increased transcript levels for cytotoxicity-associated genes (*Nkg7*, *Ctsw*; Extended Data Fig. 5b,c). This link between replicative history and a multipotency versus effector-associated gene-expression signature within the T_{CM} pool was further validated by differential gene-expression analysis and gene set enrichment analysis (Fig. 4e–g and Extended Data Fig. 5d). In line with this association, ex vivo antigen stimulation of DR+ T_{CM} cells collected from mice >60 days post *Lm*-OVA infection showed that T_{CM} cells that had undergone more prior divisions

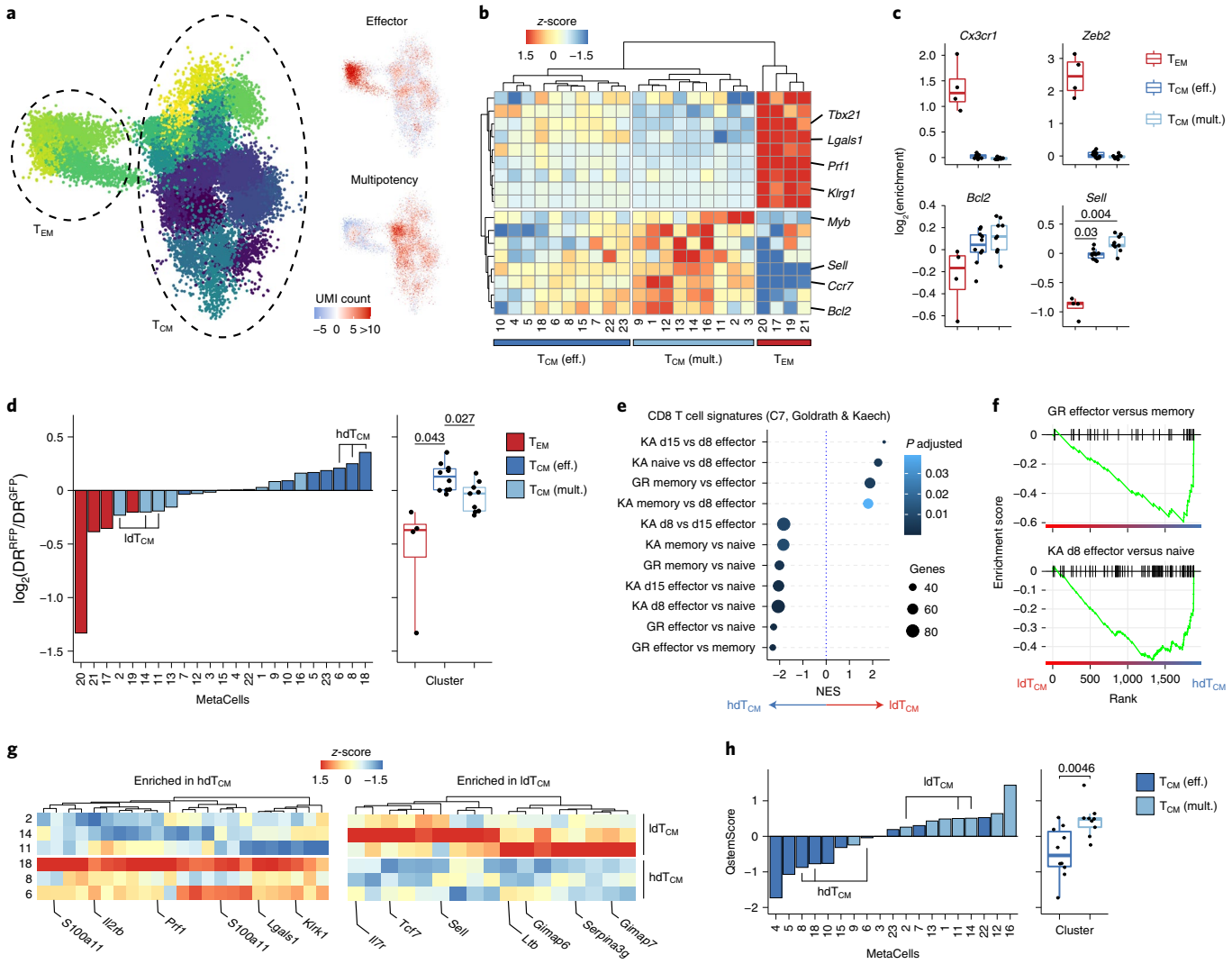

Fig. 4 | Replicative history identifies distinct transcriptional states within the T_{CM} pool. Single-cell transcriptomic profiling of DR$^+$ T cells obtained from spleen in memory phase (day 75 and day 85 after *Lm*-OVA infection)**. a**, 2D projection of all profiled cells. Colors indicate MCs (left) or relative expression of effector- and multipotency-associated genes (right). Gene list in Supplementary Table 1. **b**, Hierarchical clustering of MCs by their expression of effector- and multipotency-associated genes used in **a**. MCs are divided into three clusters on the basis of Euclidean distance. **c**, Expression of selected genes by each MC cluster. **d**, DR^{RFP}/DR^{GFP} ratio within each MC, depicted as waterfall plot (left) and boxplot (right). **e**,**f**, Enrichment of gene signatures from MSigDB (C7, collections deposited by Goldrath (GR) and Kaech (KA), Supplementary Table 2) by gene set enrichment analysis comparing ldT_{CM} and hdT_{CM} (**e**) and enrichment plots (**f**) of two representative gene sets. NES, normalized enrichment score. **g**, Heatmaps depicting genes involved in immune function that were significantly ($P < 0.05$) depleted (left) or enriched (right) within ldT_{CM} (See Extended Data Fig. 4d and Supplementary Table 3). Selected genes are annotated; complete gene lists are provided in Supplementary Table 4. **h**, QstemScore of all T_{CM} MCs depicted as waterfall plot (left) and boxplot (right). QstemScore is based on marker genes of quiescent stem cells (Supplementary Table 5)[30], see methods for calculation. Data depicted were accumulated in two independent experiments (3–4 mice per experiment). Boxplots (**c**,**d**,**h**) indicate group median and 25th and 75th percentiles, whiskers indicate the interquartile range multiplied by 1.5, and dots signify individual MCs. The phenotype clusters T_{EM}, T_{CM}(eff.), and T_{CM}(mult.) contain four, nine, and ten MCs, respectively. *P* values were determined by two-sided Tukey's HSD test (**c**), two-sided Student's *t* test with false-discovery rate correction (**d**,**h**), the FGSEA algorithm followed by the Benjamini–Hochberg procedure (**e**), or two-sided Wilcoxon rank-sum test with Bonferroni correction (**g**). Significant *P* values (< 0.05) are indicated in the plots.

were more likely to degranulate and less likely to produce IL-2 than their less divided T_{CM} counterparts (Extended Data Fig. 5e,f).

The observed divergence in replicative history between distinct T_{CM} states potentially reflects the selective quiescence of a subset of T_{CM} cells with a less differentiated state. Of note, ldT_{CM} showed reduced expression of Myc targets and genes involved in cell metabolism (Extended Data Fig. 5g), suggesting that these cells exist in a transcriptionally enforced replicative quiescent state. To test for such a transcriptional state, we scored the expression of a core gene set of quiescent stem cells from various tissues[36] (hereafter referred to as QstemScore). Notably, T_{CM} cells that showed increased expression of multipotency-associated genes were marked by a higher QstemScore than that of T_{CM} cells with increased expression of effector-associated genes (Fig. 4h). Moreover, variation in QstemScore could also be detected in gp33-specific P14 T_{CM} cells from an external dataset[37], and those P14 T_{CM} cells that prominently expressed this gene set transcriptionally resembled the multipotency-signature^{hi}effector-signature^{lo} OT-I ldT_{CM} described here (Extended Data Fig. 6). Together, these data suggest a link between T_{CM} quiescence and the expression of

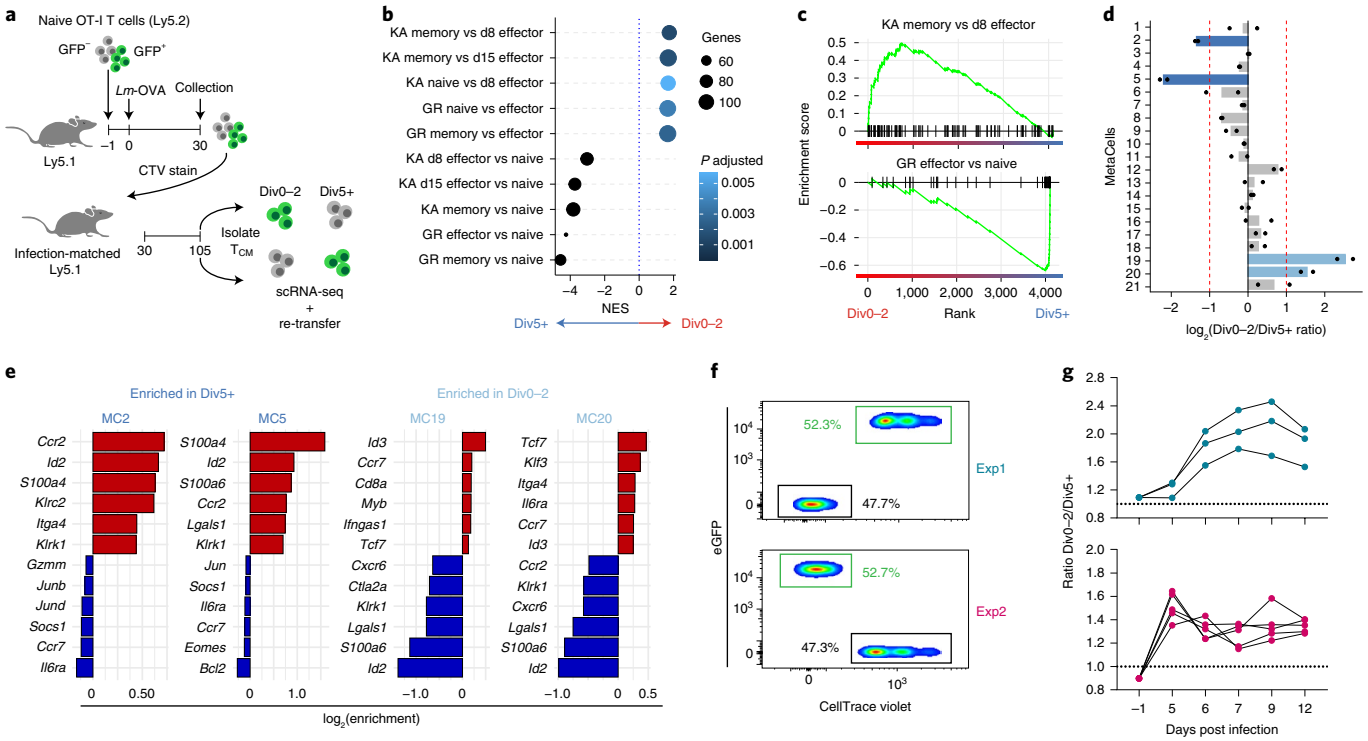

Fig. 5 | Replicative history is linked to recall potential within the T_{CM} pool. a, Experimental setup. Primary recipient mice received 5×10^5 naive OT-I and 5×10^5 naive GFP;OT-I T cells. Thirty days after *Lm*-OVA challenge, $CD8^+$ T cells were enriched, labeled with CTV, and transferred into infection-matched secondary recipient mice (one primary recipient per secondary recipient). At d105 after infection, splenic $CD27^+KLRG1^-$ T_M cells that had either divided 0–2 or 5+ times and were either GFP^+ or GFP^- were isolated by FACS. **b**, Enrichment of gene signatures from MsigDB (C7, collections deposited by Goldrath (GR) and Kaech (KA), Supplementary Table 2) between div0–2 and Div5+ cells. Top and bottom 5 pathways are depicted. **c**, Enrichment plots of representative pathways detected by gene set enrichment analysis. **d**, Ratio of normalized counts between div0–2 and div5+ cells within each MC separately calculated for GFP^+ and GFP^- populations. Bars indicate averages, dots indicate ratios of either GFP^+ or GFP^- OT-I T cells. Red dotted lines indicate a fold change of 2. **e**, Waterfall plots depicting top and bottom six marker genes for selected MCs, filtered for genes involved in immune function (Supplementary Table 3). **f**, Flow cytometry plots depicting pre-transfer mixes of div0–2 and Div5+ T_{CM} cells. **g**, T_M cells (8,000–12,000 total) as described in **f** were transferred into infection-naive mice, followed by *Lm*-OVA challenge 24 hours later. Ratios between div0–2- and div5+-derived cells were determined from peripheral blood samples at indicated days post infection. Lines connect populations from individual mice (experiment 1 $n = 3$; experiment 2 $n = 5$). Depicted scRNAseq data were collected from four mice, data describing recall potential was obtained from eight mice. *P* values were determined by the FGSEA algorithm followed by the Benjamini–Hochberg procedure (**e**).

multipotency-associated genes, driving the divergence in replicative history between distinct T_{CM} states.

To directly test whether replicative behavior in the T_{CM} pool is associated with a multipotency-associated state and relates to the functional capacity of T_{CM} to re-expand upon secondary activation, we established a DivisionRecorder-independent, CTV-based serial-transfer approach (Fig. 5a). Naive OT-I and GFP;OT-I T cells were transferred into primary recipients that were subsequently exposed to *Lm*-OVA infection. At day 30 post-infection, early T_M cells were collected, CTV-labeled, and transferred into infection-matched secondary recipients. At 75 days later, CTV^{hi} (div0–2) and CTV^{lo} (div5+) T_{CM} cells were isolated, and the resulting T_{CM} populations were then profiled by scRNAseq, or were transferred at a 1:1 ratio into tertiary recipients that were subsequently challenged with *Lm*-OVA. Strikingly, comparison of quiescent (div0–2) and proliferative (div5+) T_{CM} cells by gene set enrichment analysis revealed a clear negative association between quiescence and an effector-like transcriptional state, while quiescence was positively associated with multipotency-associated gene expression (Fig. 5b,c and Extended Data Fig. 7a). Likewise, inspection of MCs (Extended Data Fig. 7b–e) that were enriched in the div0–2 cells, showed a prominent expression of multipotency-associated genes (*Myb*, *Tcf7*, *Id3*), whereas those enriched in div5+ cells showed increased expression of effector-associated genes (*Id2*, *S00a4*, *Lgals1*) (Fig. 5d,e). Furthermore, comparison of the expansion potential of div0–2 and div5+ T_{CM} cells demonstrated that quiescent T_{CM} cells were superior in generating offspring upon renewed infection (Fig. 5f,g), further demonstrating that replicative heterogeneity in the T_{CM} pool is both linked to transcriptional state and functionality.

Re-expansion potential of T_{CM} cells is linked to prior division. Having observed a link between prior division and recall potential in adoptive transfer experiments, we set out to verify this relationship without disruption of the T_M niche, through re-challenge of recipient mice carrying DR^+ memory OT-I T cells. In case the capacity for renewed expansion would primarily be restricted to replicative quiescent T_{CM} cells, the fraction of DR^{RFP} cells should show an initial decay upon reinfection—due to the increased preponderance of offspring derived from this previously quiescent population—followed by a gradual recovery throughout the contraction phase, as a result of novel division-dependent label acquisition. Notably, analysis of the fraction of DR^{RFP} T cells in blood revealed a steep decline during the first days following secondary infection, followed by a gradual recovery during secondary memory formation (Fig. 6a and Supplementary Note 4). This transient reduction in the DR^{RFP} fraction was observed in multiple anatomical compartments (blood, spleen, liver), occurred independent of cell phenotype, and

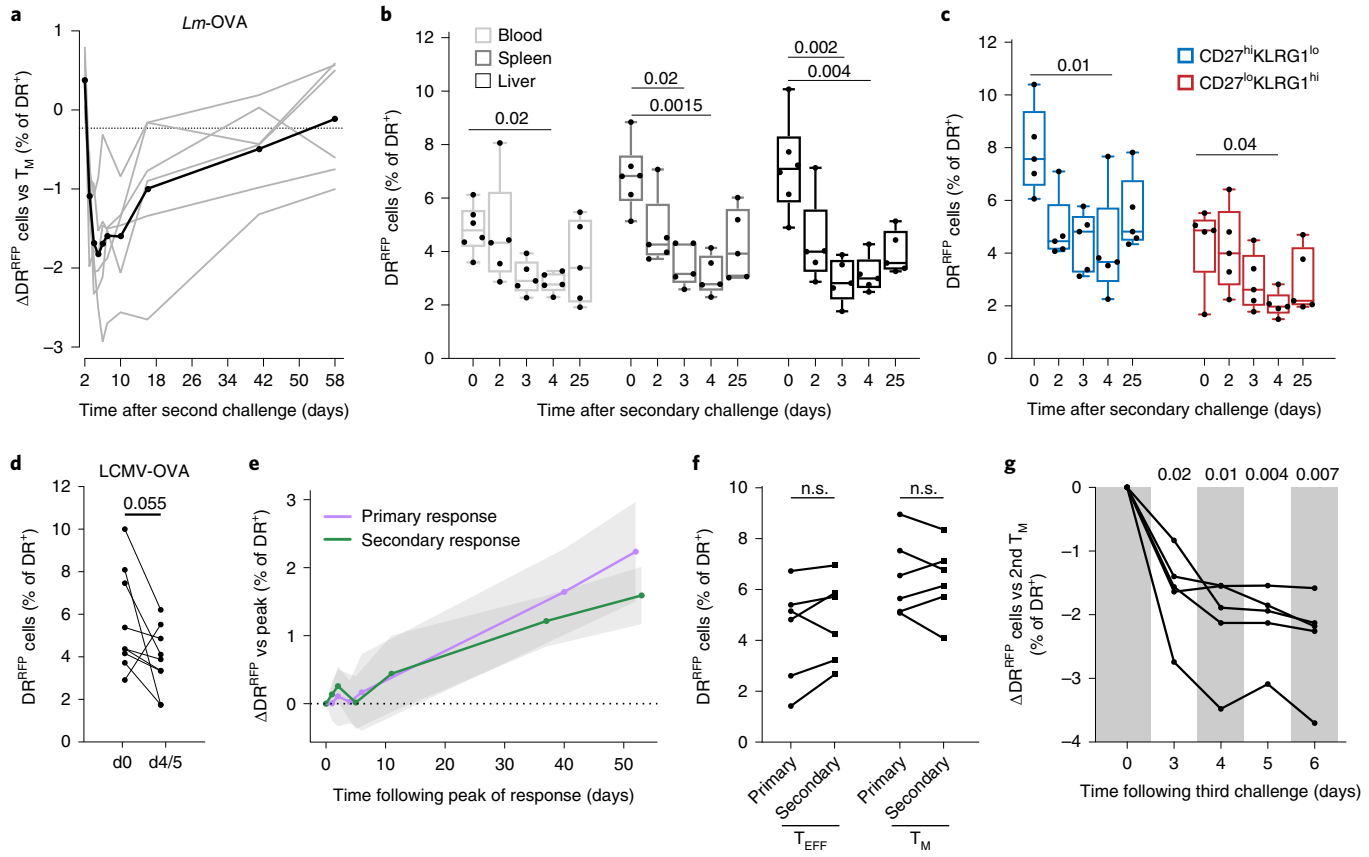

Fig. 6 | The secondary T_{EFF} pool is predominantly generated by previously quiescent memory T cells. a, Kinetics of the percentage of DR^{RFP} cells in blood upon secondary *Lm*-OVA infection. Values are relative to the DR^{RFP} percentage within the respective memory pools ($n = 6$ mice); the black line represents the group mean. **b**,**c**, DR^{RFP} percentages in the indicated organs (**b**) or within splenic $CD27^{lo}KLRG1^{hi}$ and $CD27^{hi}KLRG1^{lo}$ populations (**c**) at indicated time points ($n = 6$ mice per time point) following secondary infection. Boxplots indicate group median and 25th and 75th percentiles, whiskers represent the minimum and maximum, and dots represent individual samples. **d**, DR^{RFP} percentages in blood during the memory phase (day > 60) and at the peak of the secondary response (day 4/5 post-recall). Memory pools were generated with LCMV-OVA, recall infection was performed with *Lm*-OVA. **e**, DR^{RFP} acquisition in blood following primary and secondary infection. Values are relative to DR^{RFP} percentage at the peak of the primary or secondary response. Lines represent group medians ($n = 6$ mice per group), and grayed areas represent 95% confidence intervals. **f**, DR^{RFP} percentages in blood during effector and memory phases of the primary and secondary responses. Lines connect data from individual mice ($n = 6$). **g**, DR^{RFP} percentages in blood ($n = 5$ mice) upon tertiary infection. Mice were challenged twice with *Lm*-OVA with a >60 day interval and were subsequently infected with LCMV-OVA >60 days after secondary infection. Depicted data are representative of at least two independent experiments. *P* values were determined by two-sided Kruskal–Wallis test with Dunn's multiple-comparisons test (**b**,**c**), two-sided Wilcoxon signed-rank test (**d**,**f**), or repeated-measures one-way ANOVA followed by Dunnett correction (**g**).

was also observed in LCMV-OVA-induced T_M pools responding to secondary challenge (Fig. 6b–d). Of note, DR^{RFP} cell accumulation during the secondary contraction phase occurred at a comparable rate to that during the primary response (Fig. 6e), yielding a secondary T_M pool that—despite extensive renewed clonal expansion—had undergone a similar number of divisions as the initial memory pool (Fig. 6f, median fold difference = 1.03). Thus, the replicative histories of the T_{EFF} and T_M pools of the secondary T cell response mimic those of the primary T cell response, supporting the notion that the secondary expansion wave is mounted by a group of T_{CM} cells that has undergone limited prior division. Furthermore, this low-division T_{CM} pool is able to repeatedly reconstitute the effector T cell pool, as the same decrease in the fraction of DR^{RFP} cells was observed upon tertiary infection of mice (Fig. 6g).

To determine whether the observed data are consistent with re-expansion being driven by a T_M cell subset that becomes quiescent early in the immune response, we simulated T cell responses in which a fraction of T_{CM} precursors acquires replicative quiescence during the primary T cell response (see Supplementary Note 5 and Extended Data Fig. 8a). Specifically, T cell responses were simulated that yielded quiescent T cells at a frequency of either ~0.1% or ~1% of the T_{EFF} pool, resulting in T_M pools in which quiescent T_{CM} cells accounted for ~3% and ~25% of the memory population (Fig. 7a). Modeling of DR^{RFP} labeling rates during recall responses in which the potential to re-expand was either abruptly lost as a function of the number of prior divisions (fun 1 and 2), or was lost more gradually across division history (fun 3), demonstrated that the transient drop in DR^{RFP} fractions is consistent only with models in which the capacity to re-expand is restricted to cells that have undergone limited clonal expansion (Fig. 7b). Furthermore, the stringency of this relation is strongly dependent on the relative size of the quiescent T_{CM} pool (Fig. 7b).

Taken together, our data establish that the replicative state is not homogeneously distributed within the T_{CM} pool and is linked to distinct transcriptional and functional properties. Specifically, our observations are consistent with a dichotomy in the T_{CM} pool in which a self-renewing T_{CM} population maintains the T_M pool but marginally contributes to secondary expansion, and a replication-competent quiescent T_{CM} population is required to

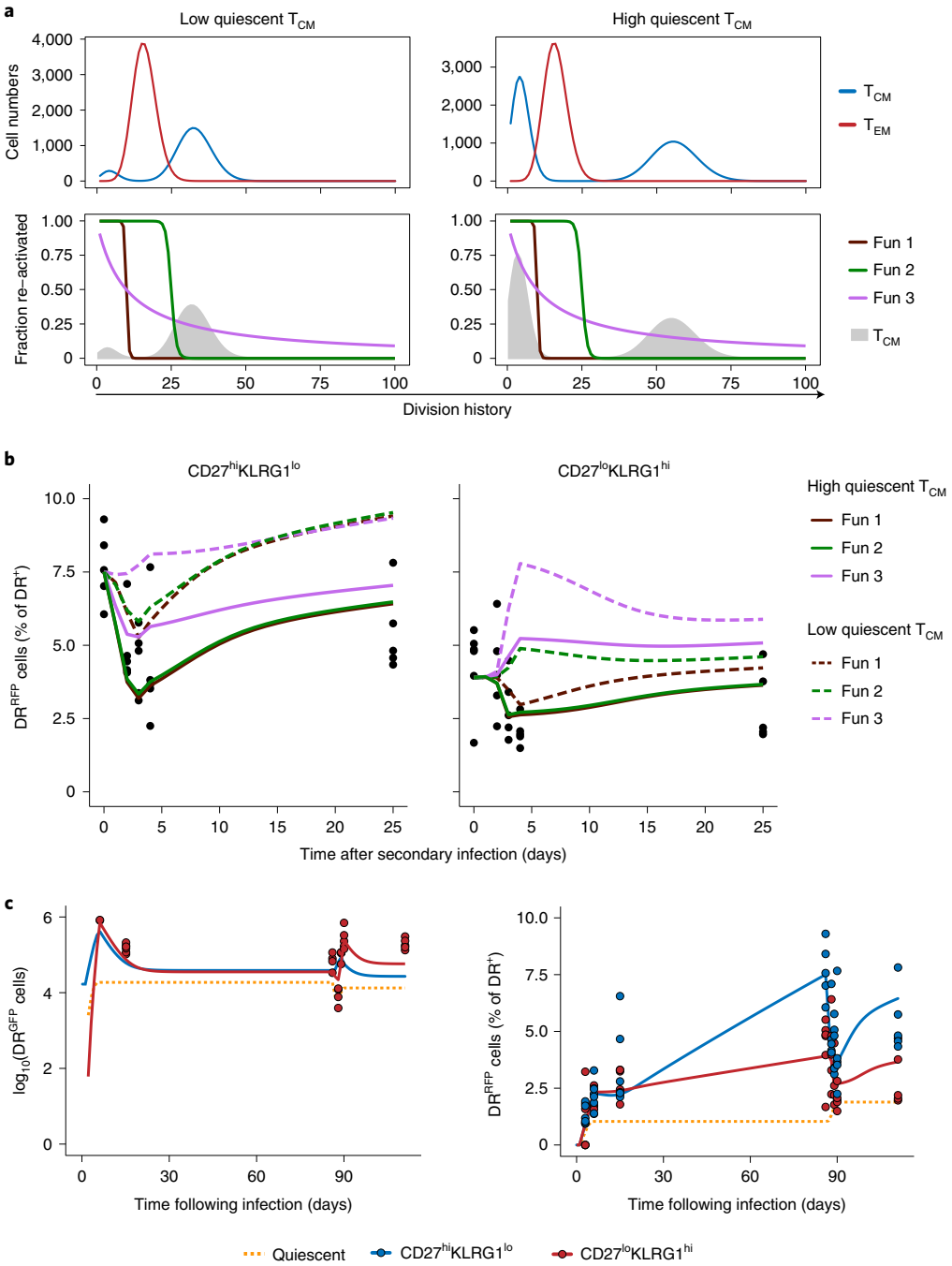

Fig. 7 | Modeled T cell responses are consistent with the presence of a replication-competent quiescent T_{CM} population. a, Division history of T_{CM} and T_{EM} pools generated by modeled T cell responses (see Supplementary Note 5) during which a high (capped at 1% of the T_{EFF} pool size) or low (capped at 0.1% of the T_{EFF} pool size) fraction of T cells acquire quiescence during the effector phase (top). 3 re-expansion functions were used to restrict which fraction of T_{CM} with a given number of prior divisions will re-expand during recall (bottom). For reference, the division history of T_{CM} is shown as a shaded area. **b**, Modeled DR^{RFP} percentages within the $CD27^{lo}KLRG1^{hi}$ and $CD27^{hi}KLRG1^{lo}$ populations during secondary responses, with each re-expansion function applied to a memory pool containing either a high or low number of quiescent T_{CM} cells. Black dots indicate experimental measurements**. j**, Best fit of the modeled T cell response (number of quiescent T cells capped to 1% of T_{EFF}) experimental data obtained from spleen, depicting either cell numbers (left) or DR^{RFP} percentages (right). See Supplementary Note 5 for details. Lines indicate the modeled populations; dots indicate experimental measurements.

form the T_{EFF} pool that arises upon renewed infection (Fig. 7c and Extended Data Figs. 8 and 9).

Discussion

Here, we report the development and application of the DivisionRecorder to dissect the replicative history of cell pools in vivo. We show that this approach allows longitudinal examination of division history, and how it may be combined with technologies such as flow cytometry and scRNAseq to couple cell state to division history. In the application presented here, the DivisionRecorder requires viral transduction to introduce one of its modules. While this did not considerably disrupt cell behavior in our study, development of a fully germline-encoded DivisionRecorder system will be attractive, for instance, to follow

replicative behavior of cell pools that are not amenable to adoptive transfer.

Using the DivisionRecorder, we demonstrate that, as a whole, the multipotent CD8$^+$ T cell pool has undergone substantial proliferation at the peak of the expansion phase, and continues to proliferate following pathogen clearance, resulting in a cumulative replicative age of the T_{CM} pool that exceeds that of the T_{EFF} and T_{EM} pool. Previous work has shown that a fraction of CD62L^{hi} precursor-T_M cells divide at a lower rate than do terminally differentiated effector subsets[10,11,32]. In line with this, we observed a lower fraction of Ki67^{hi} cells within the multipotent effector pool than in the terminally differentiated pool, early post infection. At the same time, our data indicate that this difference does not result in a reduced cumulative number of past divisions within the entire CD62L^{hi} T_{EFF} pool. Conceivably, these findings may be reconciled by the ability of highly proliferative CD62L^{lo} T_{EFF} cells to phenotypically convert to a less differentiated CD62L^{hi} state[14,15,30]. Alternatively, the precursor-T_{CM} pool may harbor a heterogeneity in replicative history that is not revealed by the phenotypic markers used.

In line with the latter possibility, by combining the DivisionRecorder with scRNAseq we reveal that, although the T_{CM} pool has undergone substantial prior division as a whole, replicative history is heterogeneous within this pool and is associated with specific transcriptional states. First, our data demonstrate the presence of T_{CM} cells that bear transcriptional similarities to T_{EM} cells but, in contrast to T_{EM} cells, remain highly proliferative in the absence of inflammation (Extended Data Fig. 9). Second, we identify a population of quiescent T_{CM} cells that expresses reduced levels of effector-associated genes, and high levels of prosurvival genes and genes associated with quiescent stem cells[36]. Several recent studies have reported the early emergence of TCF-1^{hi} and CD62L^{hi} effector cells that develop into T_M cells exhibiting stemness features[38,39]. Moreover, Johnnidis et al.[33] propose early expression of inhibitory receptors as a mechanism preserving hallmark memory features. Although these early T cell subsets bear similarities to the quiescent T_{CM} observed here, further investigations into the developmental origin of distinct T_{CM} states are necessary to better understand the lineage relationships between the T_{CM} states described here and those present during the early phases of the T cell response.

A hallmark of immunological memory is the ability to efficiently generate a new wave of T_{EFF} upon renewed infection. Our data demonstrate that this ability is predominantly confined to a subgroup of replicative nascent T_M cells. The combined observations of a less differentiated quiescent T_{CM} population, and the reconstitution of the secondary and tertiary T_{EFF} pool by the output of these nascent progenitors, make a compelling argument for the presence of a bona fide stem-cell population within the T_M pool. A growing body of work has examined a stem-cell-like T_M cell (T_{SCM}) population[40,41], generally using cell phenotype to enrich and study these cells ex vivo. Using a function-driven, phenotype-agnostic, approach that does not require removal of cells from their niche, we observe a cell behavior that fits the profile of stem-cell-like T_M cells in situ.

In high-turnover tissues, such as the bone marrow[42,43], the intestinal epithelium[44,45], and skin epidermis[46,47], two distinct behaviors of multipotent progenitor cells have been described: actively dividing cells that promote normal tissue homeostasis, and quiescent cells that have been documented to break their dormancy upon tissue injury and exhibit profound re-population capacity[42,45,48,49]. We propose that the two T_{CM} behaviors we describe provide the T cell compartment with the same capacity for renewal. Thus, the T cell pool can be viewed as an autonomous tissue that abides by organizing principles akin to those of the hematopoietic system and solid organs.

Online content

Any methods, additional references, Nature Research reporting summaries, source data, extended data, supplementary information, acknowledgements, peer review information; details of author contributions and competing interests; and statements of data and code availability are available at https://doi.org/10.1038/s41590-022-01171-9.

Received: 8 March 2021; Accepted: 24 February 2022;
Published online: 7 April 2022

References

1. Hwang, L. N., Yu, Z., Palmer, D. C. & Restifo, N. P. The in vivo expansion rate of properly stimulated transferred CD8$^+$ T cells exceeds that of an aggressively growing mouse tumor. *Cancer Res.* **66**, 1132–1138 (2006).
2. Yoon, H., Kim, T. S. & Braciale, T. J. The cell cycle time of CD8$^+$ T cells responding in vivo is controlled by the type of antigenic stimulus. *PLoS ONE* **5**, e15423 (2010).
3. Obar, J. J., Khanna, K. M. & Lefrançois, L. Endogenous naive CD8$^+$ T cell precursor frequency regulates primary and memory responses to infection. *Immunity* **28**, 859–869 (2008).
4. Blattman, J. N. et al. Estimating the precursor frequency of naive antigen-specific CD8 T cells. *J. Exp. Med.* **195**, 657–664 (2002).
5. Buchholz, V. R., Schumacher, T. N. M. & Busch, D. H. T cell fate at the single-cell level. *Annu. Rev. Immunol.* **34**, 65–92 (2016).
6. Restifo, N. P. & Gattinoni, L. Lineage relationship of effector and memory T cells. *Curr. Opin. Immunol.* **25**, 556–563 (2013).
7. Akondy, R. S. et al. Origin and differentiation of human memory CD8 T cells after vaccination. *Nature* **552**, 362–367 (2017).
8. Sarkar, S. et al. Functional and genomic profiling of effector CD8 T cell subsets with distinct memory fates. *J. Exp. Med.* **205**, 625–640 (2008).
9. Obar, J. J. & Lefrançois, L. Early signals during CD8 T cell priming regulate the generation of central memory cells. *J. Immunol.* **185**, 263–272 (2010).
10. Kretschmer, L. et al. Differential expansion of T central memory precursor and effector subsets is regulated by division speed. *Nat. Commun.* **11**, 113 (2020).
11. Kinjyo, I. et al. Real-time tracking of cell cycle progression during CD8$^+$ effector and memory T-cell differentiation. *Nat. Commun.* **6**, 6301 (2015).
12. Buchholz, V. R. et al. Disparate individual fates compose robust CD8$^+$ T cell immunity. *Science* **340**, 630–635 (2013).
13. Gerlach, C. et al. Heterogeneous differentiation patterns of individual CD8$^+$ T cells. *Science* **340**, 635–639 (2013).
14. Herndler-Brandstetter, D. et al. KLRG1$^+$ effector CD8$^+$ T Cells lose KLRG1, differentiate into all memory T cell lineages, and convey enhanced protective immunity. *Immunity* **48**, 716–729 (2018).
15. Gerlach, C. et al. The chemokine receptor CX3CR1 defines three antigen-experienced CD8 t cell subsets with distinct roles in immune surveillance and homeostasis. *Immunity* **45**, 1270–1284 (2016).
16. Reizel, Y. et al. Colon stem cell and crypt dynamics exposed by cell lineage reconstruction. *PLoS Genet.* **7**, e1002192 (2011).
17. Shlush, L. I. et al. Cell lineage analysis of acute leukemia relapse uncovers the role of replication-rate heterogeneity and microsatellite instability. *Blood* **120**, 603–612 (2012).
18. Kozar, S. et al. Continuous clonal labeling reveals small numbers of functional stem cells in intestinal crypts and adenomas. *Cell Stem Cell* **13**, 626–633 (2013).
19. Davis, F. M. et al. Single-cell lineage tracing in the mammary gland reveals stochastic clonal dispersion of stem/progenitor cell progeny. *Nat. Commun.* **7**, 13053 (2016).
20. Weber, T. S., Perié, L. & Duffy, K. R. Inferring average generation via division-linked labeling. *J. Math. Biol.* **73**, 491–523 (2016).
21. Tempany, J. C., Zhou, J. H., Hodgkin, P. D. & Bryant, V. L. Superior properties of CellTrace Yellow as a division tracking dye for human and murine lymphocytes. *Immunol. Cell Biol.* **96**, 149–159 (2018).
22. Lai, Y. The relationship between microsatellite slippage mutation rate and the number of repeat units. *Mol. Biol. Evol.* **20**, 2123–2131 (2003).
23. Koole, W., Schäfer, H. S., Agami, R., van Haaften, G. & Tijsterman, M. A versatile microsatellite instability reporter system in human cells. *Nucleic Acids Res.* **41**, e158–e158 (2013).
24. Madisen, L. et al. A robust and high-throughput Cre reporting and characterization system for the whole mouse brain. *Nat. Neurosci.* **13**, 133–140 (2010).
25. Kallert, S. M. et al. Replicating viral vector platform exploits alarmin signals for potent CD8$^+$ T cell-mediated tumour immunotherapy. *Nat. Commun.* **8**, 15327 (2017).

26. Wherry, E. J. et al. Lineage relationship and protective immunity of memory CD8 T cell subsets. *Nat. Immunol.* **4**, 225–234 (2003).
27. Becker, T. C. et al. Interleukin 15 Is required for proliferative renewal of virus-specific memory CD8 T cells. *J. Exp. Med.* **195**, 1541–1548 (2002).
28. Graef, P. et al. Serial transfer of single-cell-derived immunocompetence reveals stemness of CD8$^+$ central memory T cells. *Immunity* **41**, 116–126 (2014).
29. Olson, J. A., McDonald-Hyman, C., Jameson, S. C. & Hamilton, S. E. Effector-like CD8$^+$ T cells in the memory population mediate potent protective immunity. *Immunity* **38**, 1250–1260 (2013).
30. Youngblood, B. et al. Effector CD8 T cells dedifferentiate into long-lived memory cells. *Nature* **552**, 404–409 (2017).
31. Voehringer, D. et al. Viral infections induce abundant numbers of senescent CD8 T cells. *J. Immunol.* **167**, 4838–4843 (2001).
32. Lin, W.-H. W. et al. CD8$^+$ T lymphocyte self-renewal during effector cell determination. *Cell Rep.* **17**, 1773–1782 (2016).
33. Johnnidis, J. B. et al. Inhibitory signaling sustains a distinct early memory CD8$^+$ T cell precursor that is resistant to DNA damage. *Sci. Immunol.* **6**, eabe3702 (2021).
34. Baran, Y. et al. MetaCell: analysis of single-cell RNA-seq data using K-nn graph partitions. *Genome Biol.* **20**, 206 (2019).
35. Badovinac, V. P., Haring, J. S. & Harty, J. T. Initial T cell receptor transgenic cell precursor frequency dictates critical aspects of the CD8$^+$ T cell response to infection. *Immunity* **26**, 827–841 (2007).
36. Cheung, T. H. & Rando, T. A. Molecular regulation of stem cell quiescence. *Nat. Rev. Mol. Cell Biol.* **14**, 329–340 (2013).
37. Kurd, N. S. et al. Early precursors and molecular determinants of tissue-resident memory CD8$^+$ T lymphocytes revealed by single-cell RNA sequencing. *Sci. Immunol.* **5**, eaaz6894 (2020).
38. Grassmann, S. et al. Early emergence of T central memory precursors programs clonal dominance during chronic viral infection. *Nat. Immunol.* **21**, 1563–1573 (2020).
39. Pais Ferreira, D. et al. Central memory CD8$^+$ T cells derive from stem-like Tcf7^{hi} effector cells in the absence of cytotoxic differentiation. *Immunity* **53**, 985–1000 (2020).
40. Gattinoni, L. et al. Wnt signaling arrests effector T cell differentiation and generates CD8$^+$ memory stem cells. *Nat. Med.* **15**, 808–813 (2009).
41. Gattinoni, L. et al. A human memory T cell subset with stem cell-like properties. *Nat. Med.* **17**, 1290–1297 (2011).
42. Laurenti, E. et al. CDK6 levels regulate quiescence exit in human hematopoietic stem cells. *Cell Stem Cell* **16**, 302–313 (2015).
43. Wilson, A. et al. Hematopoietic stem cells reversibly switch from dormancy to self-renewal during homeostasis and repair. *Cell* **135**, 1118–1129 (2008).
44. Schepers, A. G., Vries, R., van den Born, M., van de Wetering, M. & Clevers, H. Lgr5 intestinal stem cells have high telomerase activity and randomly segregate their chromosomes. *EMBO J.* **30**, 1104–1109 (2011).
45. Yan, K. S. et al. The intestinal stem cell markers Bmi1 and Lgr5 identify two functionally distinct populations. *Proc. Natl Acad. Sci. USA* **109**, 466–471 (2012).
46. Clayton, E. et al. A single type of progenitor cell maintains normal epidermis. *Nature* **446**, 185–189 (2007).
47. Ito, M. et al. Stem cells in the hair follicle bulge contribute to wound repair but not to homeostasis of the epidermis. *Nat. Med.* **11**, 1351–1354 (2005).
48. An, Z. et al. A quiescent cell population replenishes mesenchymal stem cells to drive accelerated growth in mouse incisors. *Nat. Commun.* **9**, 378 (2018).
49. Sugimura, R. et al. Noncanonical Wnt signaling maintains hematopoietic stem cells in the niche. *Cell* **150**, 351–365 (2012).

Methods

DivisionRecorder vector generation. In order to prevent expression of Cre recombinase during bacterial cloning, a synthetic intron—containing a splice donor, a branch site, a pyridine rich region, and a splice acceptor—was inserted into the Cre gene through three-fragment isothermal assembly. To prevent low-level Cre translation occurring from alternative start sites, two ATG codons (position 78 and 84) were replaced by TGT codons. Finally, the Cre start codon was replaced by an EcoRI-spacer-XhoI site, to facilitate subsequent introduction of synthetic STRs. To generate the DivisionRecorder vector, two lox511 sites were introduced into the multiple cloning site of the pMX retroviral vector. Subsequently, an eGFP gene and the modified Cre recombinase gene were introduced directly upstream and downstream of the 5' lox511 site, respectively. Finally, a P2A element was inserted directly in between the eGFP gene and the 5′ Lox511 site. Together, this resulted in a cassette comprising, from 5′ to 3′: Kozak, an eGFP gene, a P2A site, a lox511 site, an EcoRI restriction site, spacer, an XhoI restriction site, a Cre recombinase gene, and a lox511 site. In its base configuration, Cre recombinase is out of frame. Synthetic STR domains were ordered as oligonucleotides (Invitrogen) and subsequently dimerized. STR dimers were inserted via the EcoRI and XhoI sites. Full sequences of all oligonucleotides are supplied in Supplementary Table 6. The retroviral expression vector of the DivisionRecorder is available from Addgene (Plasmid #179446).

Cre-activity reporter vector generation. LoxP sites were introduced into the multiple cloning site of the pCDH-CMVp-MCS-PGK-BlastR vector. In addition, a Katushka open reading frame was introduced, resulting in a vector containing from 5′ to 3′; the CMV promoter, a floxed scrambled open reading frame, a Katushka open reading frame, the PGK promoter, and a blasticidin resistance gene. The Cre-activity reporter plasmid is available from Addgene (Plasmid #179457).

Establishment of cell lines. The Cre-activity reporter cell line used in Fig. 1 was generated by retroviral transduction of HEK 293T cells (ATCC) with the Cre-activity reporter plasmid and subsequent blasticidin selection (2 µg/ml, InvivoGen). Transduced cells were seeded at 1% confluency, and resulting single cell-derived colonies were transferred to individual wells. Clones were then examined for efficiency of induction of Katushka expression upon transfection with Cre recombinase, and the best-performing clone was selected. Cre-activity reporter cells were cultured in IMDM (Gibco) supplemented with 8% FCS (Sigma), 100 U/ml penicillin (Gibco), 100 µg/ml streptomycin (Gibco), and 2 mM glutamax (Gibco). A mouse embryonic fibroblast (MEF) cell line from the Ai9 mouse strain was generated by modification of E14.5 embryonic fibroblasts with a retroviral vector encoding short-hairpin RNA directed against the p53 mRNA. Resultant cells were cultured in IMDM supplemented with 8% FCS, 100 U/ml penicillin, 100 µg/ml streptomycin, and 2 mM glutamax.

Mice. C57BL/6J-Ly5.1, OT-I, UBC-GFP, and Ai9 mice were obtained from Jackson Laboratories, and strains were maintained in the animal department of The Netherlands Cancer Institute (NKI). Ai9 and OT-I mice and UBC-GFP and OT-I mice were crossed to obtain the Ai9;OT-I and GFP;OT-I strains, respectively. Between 5–10 mice, both male and female aged 6 to 15 weeks, were used for each experiment. All animal experiments were approved by the Animal Welfare Committee of the NKI, in accordance with national guidelines.

Generation of DivisionRecorder$^+$ OT-I T cells. Platinum-E cells (Cell Biolabs) cultured in IMDM supplemented with 8% FCS, 100 U/ml penicillin, 100 µg/ml streptomycin, and 2 mM Glutamax were transfected with the DivisionRecorder vector using FuGene6 (Promega). Retroviral supernatant was collected 48 hours after transfection and stored at −80 °C. Spleens from Ai9;OT-I mice were collected and mashed through a 70-µm strainer (Falcon) into a single cell suspension, and resulting splenocytes were subsequently treated with NH_4Cl to remove erythrocytes. Subsequently, splenocytes were cultured in T cell medium (RPMI (Gibco Life Technologies) with 8% FCS, 100 U/ml penicillin, 100 µg/ml streptomycin, glutamax, 10 mM HEPES (pH 7.4), MEM non-essential amino acids (Gibco), 1 mM sodium pyruvate (Gibco), 50 µM 2-mercaptoethanol, supplemented with 1 ng/ml recombinant murine IL-7 (PeproTech) and 2 µg/mL ConcanavalinA (Merck)). After 48 hours, splenocytes were re-seeded on RetroNectin (Takara)-coated plates in T cell medium supplemented with 60 IU/mL human IL-2 and DivisionRecorder virus, and were centrifuged for 90 min at 400*g* to allow spinfection. Virus concentration was chosen such that a transduction efficiency of approximately 10–15% was achieved, in order to minimize the occurrence of multiple retroviral integrations (Supplementary Note 6). Cells were collected 24 hours later, and a small aliquot was stained with anti-CD8-PercpCy5.5, anti-Vb5-PeCy7, anti-CD45.2-AF700, and DAPI to determine the fraction of viable OT-I T cells (DAPI$^-$CD8$^+$Vb5$^+$CD45.2$^+$) by flow cytometry (Fortessa, BD Bioscience), which generally was around ~80%. CD8$^+$Vb5$^+$CD45.2$^+$ cells that expressed GFP were considered DivisionRecorder$^+$ OT-I cells. Within the initial population of DivisionRecorder$^+$ OT-I cells, the fraction of cells that already showed reporter activation (as inferred by tdTomato expression) 24 hours after transduction was consistently between 0.4 and 0.8%. Activated splenocytes were prepared for adoptive transfer (see below).

Infection, adoptive transfer and cell recovery. C57BL/6J-Ly5.1 mice were infected with 5,000–10,000 CFU of a recombinant *Listeria monocytogenes* strain that expresses ovalbumin or with 5,000 PFU artLCMV-OVA[25]. Approximately 24 hours later, infected mice received 5,000-40,000 DivisionRecorder$^+$ OT-I T cells through intravenous tail vein injection. For secondary challenge experiments, mice were infected with a 10-fold higher *Lm*-OVA dose compared to primary infection (that is, 50,000–100,000 CFU) at indicated time points. To analyze OT-I T cell responses in peripheral blood over time, 25- to 50-µL blood samples were obtained from the tail vein at the indicated time points, and were treated with NH_4Cl supplemented with 0.2 mg/ml grade-II DNaseI (Roche) to remove erythrocytes (see 'Flow cytometric analysis'). To obtain spleen and liver samples, mice were euthanized, organs were collected, and single-cell suspensions were prepared by means of mashing through a 100-µM or 70-µm strainer (Falcon), respectively. Subsequently, erythrocytes were removed by treatment with NH_4Cl. To purify leukocytes from single-cell suspensions of liver tissue, cell suspensions were separated over a 37.5% Percoll (Sigma) density gradient. Obtained blood, spleen, and liver samples were further processed for flow cytometric analysis, scRNAseq or functional in vitro assays, as indicated. Samples were monitored for the occurrence of retroviral silencing, which was not observed in any of the examined samples (Supplementary Note 7).

Validation of DivisionRecorder functionality. To assess the ability of the DivisionRecorder to faithfully report on the replicative history of T cell populations using dilution of cell dyes as a reference, as described in Fig. 2d,e, we employed an experimental approach that was optimized to obtain sufficient DR^{RFP} events within the limited number of cell divisions that can be followed using cell dyes such as CTV (that is, by transferring a high number of cells modified at a high transduction efficiency). Conclusions from this experiment are restricted to the validation of the functionality of the DivisionRecorder in dividing CD8$^+$ T cells. Splenic CD8$^+$ T cells were isolated using the Mouse CD8 T Lymphocyte Enrichment Set (BD Biosciences) and were subsequently stained with CellTrace Violet (Thermo Fisher). Next, cells were activated for 16 hours in T cell medium supplemented with 0.05 µg/mL SIINFEKL peptide and 60 IU/ml IL-2. Following this activation step, cells were seeded onto RetroNectin (Takara Bio)-coated plates and were transduced with DivisionRecorder virus by spinfection for 4 hours in the presence of IL-2 and SIINFEKL peptide. Analysis of CellTrace Violet signal by flow cytometry indicated that the cells had not undergone a full cell division post labeling. Subsequently, 6×10^6 OT-I T cells were transferred into *Lm*-OVA infected recipients. Spleens were collected 48 hours after adoptive transfer, processed into single-cell suspensions, and prepared for flow cytometric analysis. In order to accurately determine the fraction of DR^{RFP} cells per division during the initial stages of the proliferative burst when cumulative switching rate is still low, analysis of a large number of DivisionRecorder$^+$ OT-I T cells events is required. For this reason, a transduction efficiency of ~60% was chosen in these experiments, instead of the 10–15% transduction efficiency used in other experiments. Note that a high transduction efficiency will result in the more frequent occurrence of cells that carry multiple retroviral integrations. The presence of cells with multiple integrations will result in a higher, yet stable, DR^{RFP} acquisition rate, as compared with the experimental setup used in the remainder of the study.

Ex vivo analysis of degranulation and cytokine secretion potential of T_M cells. Spleens were collected from recipient mice at >60 days post-infection, and CD8 T cells were isolated using the Mouse CD8 T Lymphocyte Enrichment Set (BD Biosciences). Following isolation, T cells were plated at 1×10^6 cells per well in 96-well round bottom plates in T cell medium supplemented with 0.05 µg/mL SIINFEKL peptide to selectively activate OVA-specific T cells. Following a 4 hour incubation, the capacity of indicated T cell populations to either produce the indicated cytokines or to degranulate was assessed. To allow analysis of cytokine production, Brefeldin A (GolgiPlug, BD Biosciences) was added 30 minutes after initiation of T cell stimulation. To allow analysis of degranulation, T cell medium was supplemented with anti-CD107a and anti-CD107b antibodies at the initiation of T cell stimulation, and Brefeldin A (GolgiPlug, BD Biosciences) and Monensin (GolgiStop, BD Biosciences) were added 30 minutes after initiation of T cell stimulation. At the end of the T cell stimulation period, cells were stained for KLRG1 and CD27 and prepared for flow cytometric analysis (see below).

Flow cytometric analysis. Cells were taken up in PBS (Invitrogen) supplemented with 0.5% BSA (Fisher Scientific), and stained with antibodies directed against the indicated cell surface proteins (1:200 dilution), for 30 minutes on ice. To allow detection of intracellular cytokine production, cells were fixed and permeabilized with CytoFix/CytoPerm (BD Biosciences) according to the manufacturer's protocol and were subsequently stained using antibodies against IL-2, TNFα, and IFNγ. To detect intranuclear Ki67 expression, the Foxp3/Transcription factor Staining buffer set (eBioscience) was used. See Supplementary Table 7 for a list of antibodies used in the study. All samples were acquired on a BD LSR Fortessa (BD Bioscience); DR^{GFP} and DR^{RFP} cells were identified as CD8$^+$Vβ5$^+$CD45.2$^+$GFP$^+$tdTomato$^-$ and CD8$^+$Vβ5$^+$CD45.2$^+$GFP$^+$tdTomato$^+$, respectively. Flow cytometry data analysis was performed using FlowJo V10. An example of the used gating strategy is depicted in Extended Data Fig. 10.

For the moving average analysis depicted in Fig. 3g and Extended Data Fig. 2e, $CD8^+V\beta5^+CD45.2^+GFP^+$ events were exported and further processed using the R package FlowCore[50]. In brief, outlier events (that is, antibody aggregates/cell doublets) were removed, fluorescence intensities of each of the cell surface proteins were normalized using an inverse hyperbolic sine transformation and subsequently scaled between 0 and 1. To obtain the depicted moving averages, the fraction of DR^{RFP} cells was calculated within windows that each contained 10% of total cells, starting with the 10% of cells with the lowest expression levels for the indicated marker, and with subsequent windows moving up by steps of 2.5%.

Single-cell RNA sequencing and data analysis of DivisionRecorder modified cells. The scRNAseq dataset of DivisionRecorder modified and unmodified OT-I T_M cells was obtained in two independent experiments, comprising 11 mice in total (See Extended Data Fig. 3). Experiment 1 included 3 mice containing DR^+ T_M cells (mouse 1–3), which were processed in a single batch. Experiment 2 included 4 mice containing DR^+ T_M cells (mouse 4–7), and 4 mice containing T_M cells derived from naive OT-I T cells (unmodified, mouse 8–11), which were processed in two separate batches (batch 1: mouse 4–5 and mouse 8–9, batch 2: mouse 6–7 and mouse 10–11).

Spleens of mice that received DivisionRecorder$^+$ OT-I T cells ($n=7$) or mice that received naive OT-I T cells ($n=4$) were collected >65 days following infection. Splenocytes were stained with fluorochrome-conjugated antibodies directed against CD8, CD45.2, and Vβ5 (see Supplementary Table 7), to allow purification of transferred cells by FACS using the BD FACSAria Fusion Flow Cytometer (BD Biosciences). DR^+ cells were subsequently FACS purified on the basis of their expression of RFP and GFP. Following the isolation of DR^{GFP} and DR^{RFP} T_M cells by FACS (FACSAria Fusion, BD Biosciences), obtained cell populations were barcode-labeled with distinct anti-mouse TotalSeq Hashtag antibodies (TotalSeq-A0301–0306, Biolegend) and pooled, with an equal number of cells from each mouse to form the total pool of cells for scRNAseq. If the amount of sorted DR^{RFP} cells from a particular sample was limited, it was pooled together with another DR^{RFP} sample to reduce cell loss during cell hashing (as indicated in Extended Data Fig. 3). Single-cell RNA isolation and library preparation was performed according to the manufacturer's protocol of the 10X Genomics Chromium Single Cell 3′ kit, and the cDNA library was sequenced on a NextSeq 550 Sequencing System (Illumina). Cumulative data tallied to a total of ~39,500 cells. Feature-barcode matrices were generated using the Cell Ranger software of the 10X Genomics Chromium pipeline. Cells that could be ascribed to multiple samples or to no sample (inferred from the detection of multiple or no Hash tags), cells with a transcript (UMI) count lower than 1,500 and cells with a mitochondrial-gene fraction higher than 0.12 were excluded from downstream analysis. Next, cells were further filtered on the basis of gene counts, setting upper and lower thresholds separately for each sample-batch to control for differences in sequencing depth (gene-count thresholds: experiment 1, 1,200–3,000; experiment 2 batch 1, 800–2,500; experiment 2 batch 2, 1,000–3,000). Subsequent analysis of the remaining 27,559 cells was performed using the Seurat[51] and MetaCell[34] R packages.

To examine enrichment or depletion of DR^{RFP} cells within the different MetaCells, cell counts were first normalized across hashtags. Data obtained from the different mice were subsequently aggregated and used to calculate the ratio of DR^{RFP} versus DR^{GFP} cells in each MetaCell. The immune signature gene list used in several analyses was composed of gene clusters involved, or proposed to be involved, in T cell function. The full gene list is described in Supplementary Table 3.

Differential gene-expression testing was performed using the FindMarkers function (Wilcoxon rank-sum test) implemented in Seurat, comparing all ldT_{CM} to all hdT_{CM}. Significantly differentially expressed genes ($P<0.05$) were subsequently used for gene-set enrichment analysis using the R package fgsea[52], testing for enriched gene-sets from the C7 immunologic or the H Hallmark gene-sets from Molecular Signatures Database (only including sets that consisted of >10 genes). Results from this analysis were filtered for collections deposited by Kaech and Goldrath (Supplementary Table 2), focusing on relevant $CD8^+$ T cell biology.

To calculate the QstemScore, the $\log_2$ enrichment values of genes that were positively or negatively associated with stem cell quiescence (Supplementary Table 5) were first summed within each MetaCell, resulting in a positive and a negative score. QstemScore was then obtained by subtracting the negative score from the positive score.

Re-analysis of LCMV-specific T_M cell scRNAseq dataset. Single-cell transcriptomes from P14 T_M cells (collected from spleen at day 90 post infection) were obtained from the Gene Expression Omnibus (accession GSE131847, sample GSM3822202). All single cells from this dataset were clustered by applying the MetaCell algorithm. Next, T_{CM} MetaCells were determined on the basis of the expression levels of core effector- and multipotency-related genes (Supplementary Table 1). QstemScores were then calculated for each of the T_{CM} MetaCells, and the two highest- and two lowest-scoring MetaCells were selected. Pearson correlations were subsequently calculated between each of these four T_{CM} MetaCells, and all of the T_{CM} MetaCells from the OT-I dataset described here.

CTV-based serial transfer experiment and analysis. Spleens from OT-I and GFP;OT-I mice were collected and $CD8^+$ T cells were isolated using the Mouse CD8 T Lymphocyte Enrichment Set (BD Biosciences), according to the manufacturer's protocol. The obtained cells were mixed in a 1:1 ratio and transferred to 4 primary recipient C57BL/6J-Ly5.1 mice (1.5×10^6 T cells per recipient), and 24 hours later recipients were infected with 5,000–10,000 CFU *Lm*-OVA. At 30 days following infection, spleens and lymph nodes were collected, and $CD8^+$ T cells were enriched using the Mouse CD8 T Lymphocyte Enrichment Set (BD Biosciences), replacing the supplied antibody-cocktail with a mixture of anti-mouse CD19, CD20, and CD4 biotinylated antibodies (used 1:200 each, see Supplementary Table 7 for information on antibody clones). The enriched cell pool was subsequently stained with CellTrace Violet (Thermo Fisher) and re-transferred into four infection-matched secondary C57BL/6J-Ly5.1 recipients. At 74 days after secondary transfer (104 days post-infection), spleens and lymph nodes were collected from the secondary recipients and stained with anti-mouse KLRG1-PE, CD27-APC, and CD45.2-AF700 (See Supplementary Table 7 for information on antibody clones). Next, stained cell pools were first enriched for transferred cells (that is, $CD45.2^+$) through FACS using the BD FACSAria Fusion Flow Cytometer (BD Biosciences), and subsequently sorted again to obtain 4 populations of T_{CM} cells based on both GFP expression and CTV dilution: $KLRG1^-CD27^+GFP^+$div0–2, $KLRG1^-CD27^+GFP^+$div5+, $KLRG1^-CD27^+GFP^-$div0–2, and $KLRG1^-CD27^+GFP^-$div5+. These cell pools were then further processed for tertiary transfer or single-cell RNA sequencing.

For tertiary transfer, GFP^-div0–2 cells were mixed 1:1 with the GFP^+div5+ cells (experiment 1), or GFP^+div0–2 cells were mixed 1:1 with GFP^-div5+ cells (experiment 2), thereby controlling for potential confounding effects of the donor strain. Next, 10,000 cells from each cell pool were transferred in naive tertiary recipient C57BL/6J-Ly5.1 mice (3 mice for experiment 1, 4 mice for experiment 2). Twenty-four hours later, recipients were infected with 10,000 CFU *Lm*-OVA, and the ratio of GFP^+ to GFP^- cells within the transferred population ($Ly5.2^+$) in blood was monitored by flow cytometry over time.

For scRNAseq analysis, cell pools obtained by cell-sorting were barcode-labeled with distinct anti-mouse TotalSeq Hashtag antibodies (TotalSeq-A0301-0304, Biolegend) and subsequently pooled. Single-cell mRNA isolation and library preparation was performed according to the manufacturer's protocol of the 10X Genomics Chromium Single Cell 3' kit, and the cDNA library was sequenced on a NextSeq 550 Sequencing System (Illumina). Feature-barcode matrices were generated using the Cell Ranger software of the 10X Genomics Chromium pipeline, resulting in 13,064 single-cell transcriptomes. Cells that could be ascribed to multiple samples or to no sample (inferred from the detection of multiple or no hashtags), cells with a transcript (UMI) count lower than 2,000, and cells with a mitochondrial-gene fraction higher than 0.12 were excluded from downstream analysis. Finally, cells with a gene-count of >2,800 were additionally excluded from further analysis. Subsequent analysis of the remaining 9,702 cells was performed using the Seurat[51] and MetaCell[34] R packages.

Differential gene-expression testing was performed using the FindMarkers function (Wilcoxon rank-sum test) implemented in Seurat, comparing all CTV^{hi} (div0–2) cells to all CTV^{lo} (div5+) cells. Significantly differentially expressed genes ($P<0.05$) were subsequently used for gene-set enrichment analysis using the R package fgsea[52], testing for enriched gene-sets from the C7 immunologic gene-sets (including only sets that consisted of >10 genes). Results from this analysis were filtered for collections deposited by Kaech and Goldrath (Supplementary Table 2), focusing on relevant $CD8^+$ T cell biology.

For the MetaCell-based analysis, the number of cells within each hashtag-MetaCell combination was counted, and subsequently normalized to 1,000 cells within each hashtag. The ratio of CTV^{hi} to CTV^{lo} was then calculated separately for the GFP;OT-I- and OT-I-derived cells.

Statistical analysis. Flow cytometric data were acquired using BDFACSDiva (v8.0) software. Flow cytometric data were analyzed using Flowjo (v10.4.2), R (v6.3.1, 'Action of the Toes'), and FlowCore (v1.52.1). Single-cell RNA sequencing data were analyzed using R (v 6.3.1), Seurat (v3.1.1), and MetaCell (v0.3.41). Data were visualized using Graphpad (V8.4.1, Prism software) and GGplot (v3.2.1). No statistical methods were used to predetermine sample sizes, and sample sizes were chosen on the basis of those reported in previous publications[13,53]. Data distribution was assumed to be normal, but this was not formally tested. Mice were stratified according to age and sex where appropriate. Data collection and analysis were not performed blind to the conditions of the experiments. No data points were excluded from the analyses.

Reporting Summary. Further information on research design is available in the Nature Research Reporting Summary linked to this article.

Data availability

Transcriptomic data presented in the manuscript have been deposited to the Gene Expression Omnibus (GEO), and can be accessed under the GEO accession numbers GSE169154 and GSE184947. The gp33-specific P14 T cell scRNAseq dataset was retrieved from GEO (accession GSE131847, sample GSM3822202). All statistical source data of the figures presented in the present study are provided with this paper. Indicated gene sets used in gene set enrichment analyses were retrieved from the Molecular Signatures Database (MSigDB) at http://www.gsea-msigdb.org/gsea/msigdb. Any additional data supporting the findings of this

study are available from the corresponding authors upon request. Source data are provided with this paper.

Code availability

R scripts that were used to produce the main and extended data figures in the manuscript are available from GitHub (https://github.com/kasbress/DivisionRecorder_analysis).

References

50. Hahne, F. et al. flowCore: a Bioconductor package for high throughput flow cytometry. *BMC Bioinforma.* **10**, 106 (2009).
51. Butler, A., Hoffman, P., Smibert, P., Papalexi, E. & Satija, R. Integrating single-cell transcriptomic data across different conditions, technologies, and species. *Nat. Biotechnol.* **36**, 411–420 (2018).
52. Korotkevich, G. et al. Fast gene set enrichment analysis. Preprint at bioRxiv / https://doi.org/10.1101/060012 (2016).
53. Kok, L. et al. A committed tissue-resident memory T cell precursor within the circulating CD8$^+$ effector T cell pool. *J. Exp. Med.* **217**, e20191711 (2020).

Acknowledgements

We would like to thank M. C. Wolkers (Sanquin, Amsterdam), C. Gerlach (Karolinska Institute, Stockholm), and K. van Gisbergen (Sanquin, Amsterdam) for helpful discussions regarding experimental procedures and sharing biological material, and D. Merkler (University of Geneva, Geneva) for kindly providing the artLCMV-OVA. In addition, we would like to thank the NKI Genomics Core Facility and Flow Cytometry Core Facility for providing experimental support. This work was supported by ERC AdG Life-his-T (Grant agreement ID: 268733) to T.N.S. and an NWO grant (ALWOP.265) to R.J.d.B.

Author contributions

The study was designed by K.B., L.K., F.A.S. and T.N.S., and was supervised by T.N.S. and F.A.S.; K.B. and L.K. jointly performed, analyzed, and visualized all experimental work included in the manuscript; F.A.S. and K.B. designed and developed the retroviral DivsionRecorder construct. L.A.K. and L.J. performed optimization and validation experiments integral to the design of the DivisionRecorder; A.C.S. and R.J.d.B. performed mathematical modeling, together with T.S.W., L.P. and K.R.D.; K.B. and L.K. wrote the manuscript with the input of co-authors; T.N.S. and F.A.S. critically reviewed and revised the manuscript.

Competing interests

The authors declare no competing interests.

Additional information

Extended data is available for this paper at https://doi.org/10.1038/s41590-022-01171-9.

Supplementary information The online version contains supplementary material available at https://doi.org/10.1038/s41590-022-01171-9.

Correspondence and requests for materials should be addressed to Ferenc A. Scheeren or Ton N. Schumacher.

Peer review information *Nature Immunology* thanks Mohamed Abdel-Hakeem and the other, anonymous, reviewer(s) for their contribution to the peer review of this work. L. A. Dempsey was the primary editor on this article and managed its editorial process and peer review in collaboration with the rest of the editorial team. Peer reviewer reports are available.

Reprints and permissions information is available at www.nature.com/reprints.

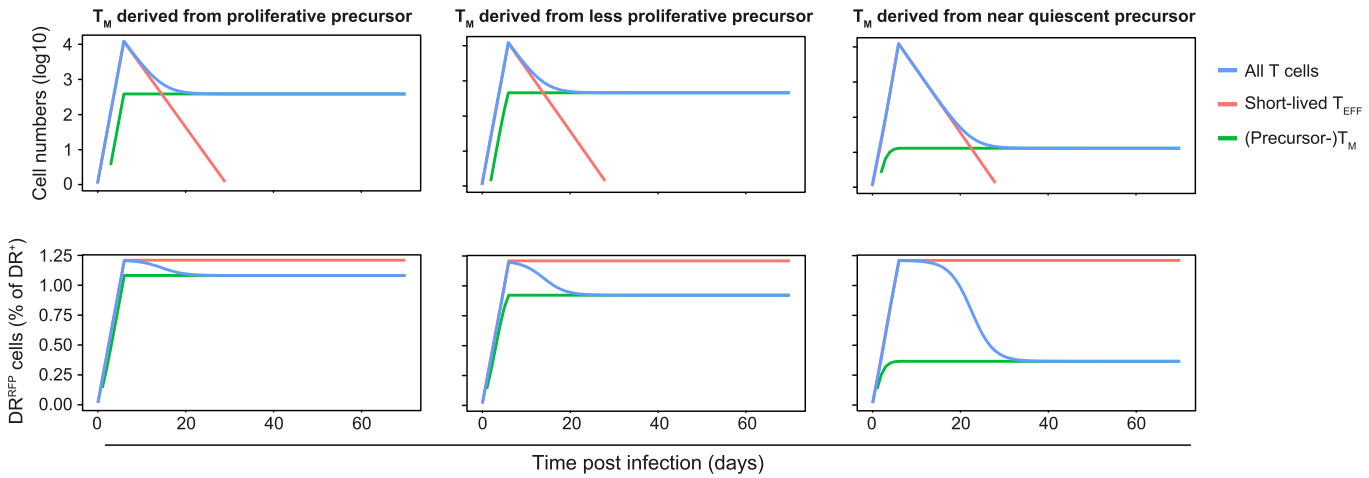

Extended Data Fig. 1 | Simulation of different scenarios of memory T cell formation. Simulated data depicting a responding antigen-specific T cell population (blue), comprised of T_{EFF} undergoing clonal expansion and subsequent contraction (red), plus memory precursor T cells (MP, green) that develop into T_M. Activated T_{EFF} are modeled to divide rapidly for 6 days (expansion phase), die at a fixed rate throughout the response, and can differentiate into MP cells only during the expansion phase. Cell numbers (top row) and DR^{RFP} percentages (bottom row) are shown for 3 scenarios: (left) T_{EFF} can give rise to MP cells during the entire expansion phase, irrespective of the number of prior divisions, (middle) only T_{EFF} that have gone through at most 24 divisions can give rise to MP cells, or (right) only T_{EFF} that have gone through at most 10 divisions can give rise to MP cells. Note the strong decay in DR^{RFP} percentage that is observed during memory formation in case T cell memory is founded by T cells that have undergone few divisions. See Supplementary Note 3 for detailed description and equations.

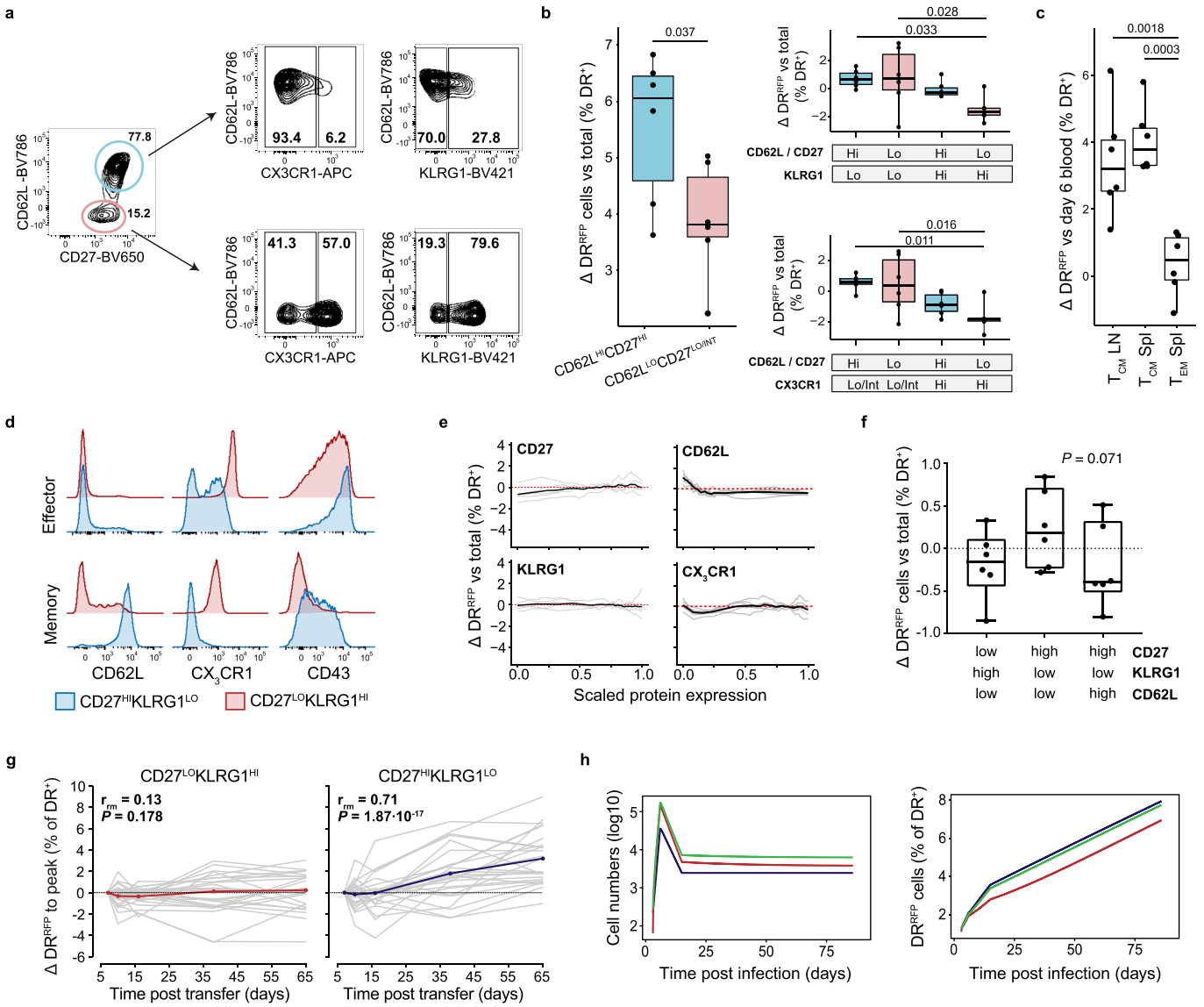

Extended Data Fig. 2 | Evaluation of the division history of T cell subsets throughout a response to *Lm*-OVA. a, Gating strategy used to identify indicated T_M populations (d86) in spleen samples. **b**, DR^{RFP} percentages within splenic T_M populations (n = 6 mice) as identified in panel a. **c**, DR^{RFP} percentages within the $CD27^{HI}KLRG1^{LO}$ T_{CM} subset in spleen and lymph nodes (LN) and within the $CD27^{LO}KLRG1^{HI}$ T_{EM} subset in spleen. **d**, Cell surface expression of CX_3CR1, CD62L, and CD43 within splenic $CD27^{LO}KLRG1^{HI}$ and $CD27^{HI}KLRG1^{LO}$ populations at the peak of the T_{EFF} phase (day 6 post infection) and in memory phase (day 86 post infection). **e**, Moving-average of surface marker expression of splenic DR^+ OT-I T cells during effector phase (day 6), depicted as in Fig. 3g. **f**, Boxplots depicting DR^{RFP} percentages within T_{EFF} (day 6 post infection) subsets in spleen (n = 6 mice), relative to the total DR^{RFP} percentage. **g**, Kinetics of DR^{RFP} percentages within $CD27^{LO}KLRG1^{HI}$ (left) and $CD27^{HI}KLRG1^{LO}$ (right) DR^+ OT-I T cell populations in blood. Values are relative to the percentage of DR^{RFP} cells detected at the peak of the response (day 6). Grey lines represent individual mice (n = 22), red and blue lines indicate group mean. **h**, Simulation of the phenotype model (See Supplementary Note 5 for details) illustrating a scenario in which conversion of $CD27^{HI}KLRG1^{LO}$ to $CD27^{LO}KLRG1^{HI}$ cells occur only after the peak of the response at a low rate. Depicted are the overall cell numbers (left), and the percentage DR^{RFP} cells of DR^+ OT-I T cells (right) in $CD27^{HI}KLRG1^{LO}$ cells (blue), $CD27^{LO}KLRG1^{HI}$ cells (red) and the total T cell population (green). Note that in this scenario the fraction DR^{RFP} within the terminally differentiated $CD27^{LO}KLRG1^{HI}$ population would increase to almost twice the experimentally observed frequency. All depicted data are representative of at least two independent experiments. Boxplots (**c, d, g**) represent group median and 25^{th}/75^{th} percentiles, whiskers indicate the interquartile range multiplied by 1.5 (**c, d**) or min/max (**g**), dots indicate individual samples. *P* values were determined by one-way ANOVA followed by Tukey's HSD post-hoc test (**c** and **d**), two-sided Student's T test (**c**), two-sided repeated measurement correlation test (**h**), or two-sided Friedman test (**g**). All significant (< 0.05) P values are indicated in the plots.

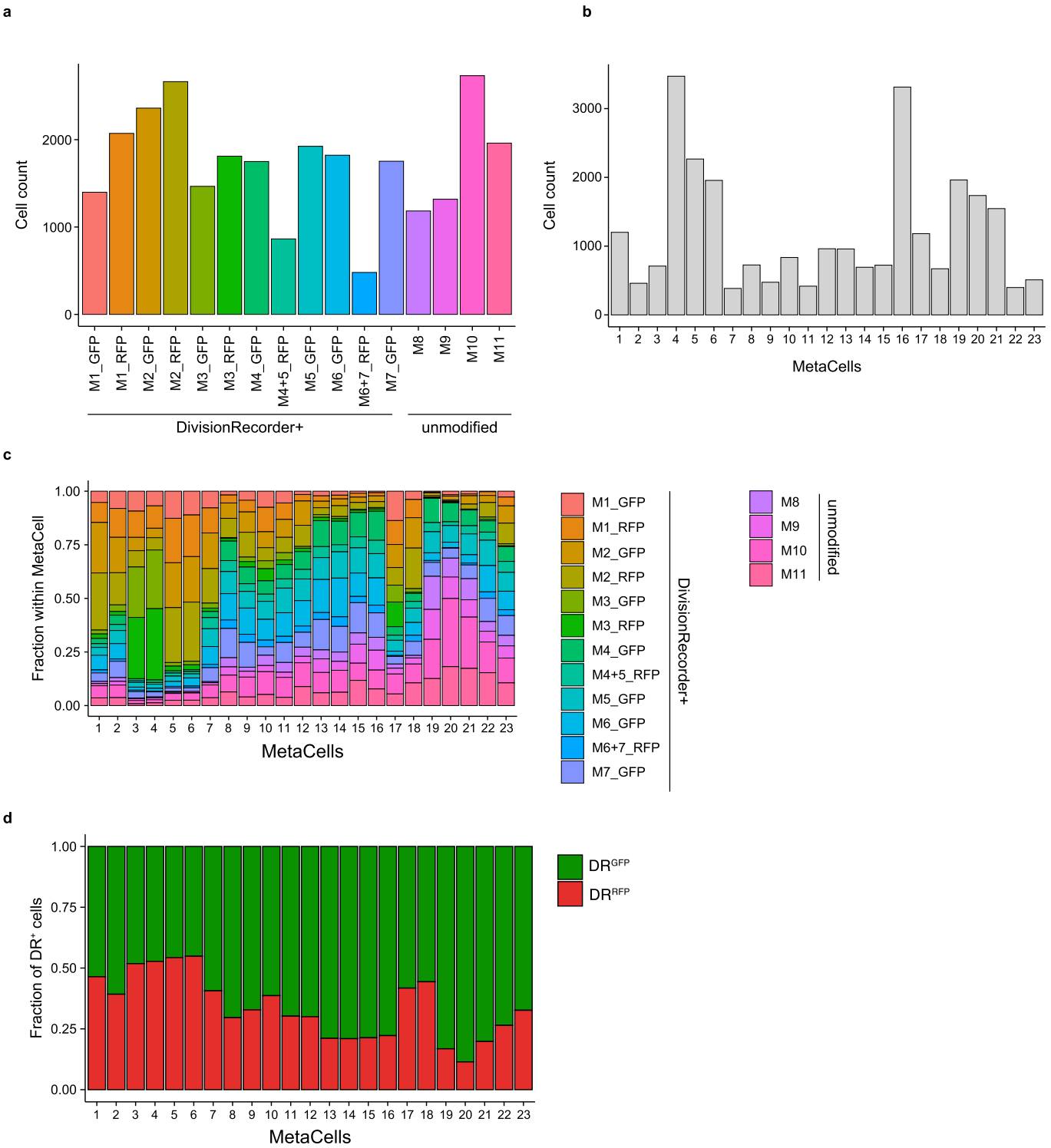

Extended Data Fig. 3 | Single cell mRNA sequencing of DivisionRecorder$^+$ and unmodified memory T cells. Single cell mRNA sequencing was performed on DivisionRecorder modified and unmodified OT-I memory T cells (Day 75 and 85 post *Lm*-OVA infection), isolated from spleens (n = 7 mice with DR + memory T cells; n = 4 with unmodified memory T cells). Obtained data were aggregated from two independent experiments (Experiment 1: M1$^-$3; Experiment 2: M4-11). All cells were jointly analysed and clustered. **a**, Cell count per sample. **b**, Total cell count per MC. **c**, Sample composition of each MC. **d**, Relative contribution of DR^{GFP} and DR^{RFP} to the total DR$^+$ pool within each MC.

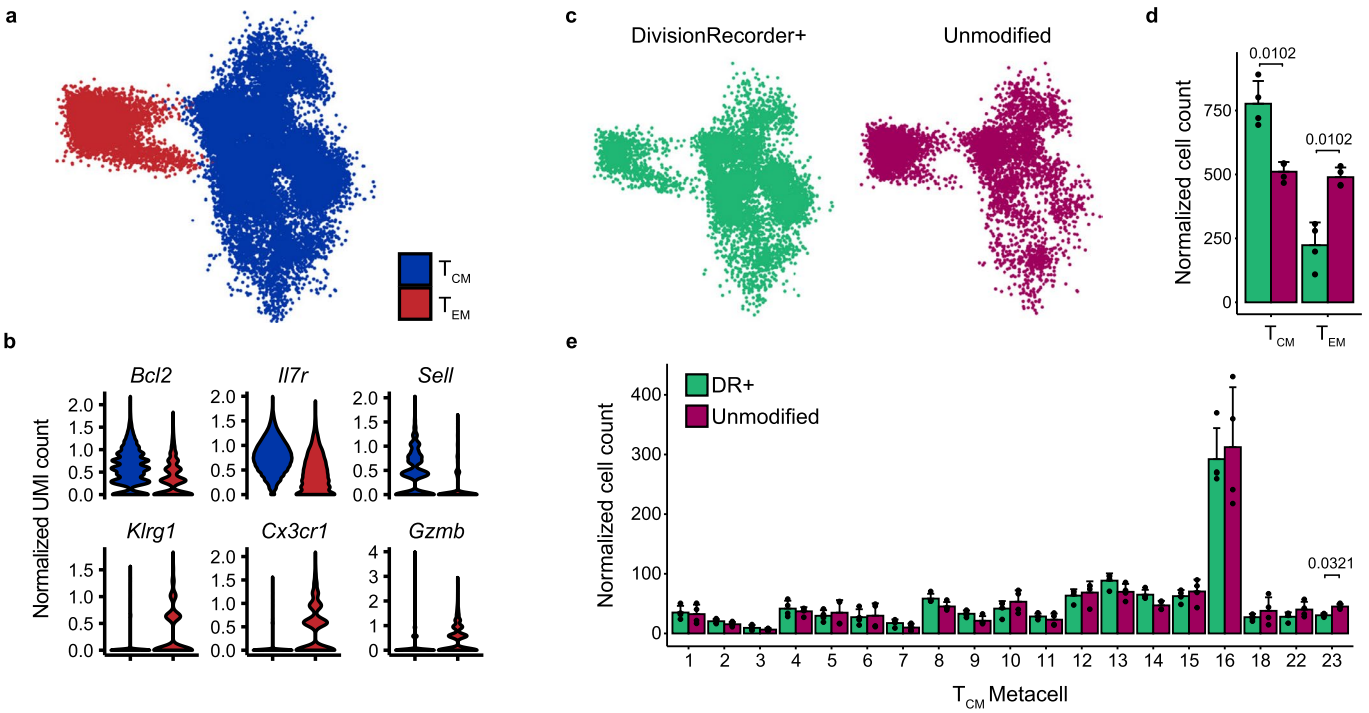

Extended Data Fig. 4 | T_{CM} transcriptional states are preserved in DR$^+$ OT-I T cells. Comparison of transcriptional states of splenic memory T cells generated by either DivisionRecorder modified, or unmodified OT-I T cells (Day 75 and 85 post *Lm*-OVA infection). **a-b**, Memory OT-I T cells cluster into T_{CM} (blue) and T_{EM} (red). 2D projection colored by subset (**a**), and violin plots depicting normalized UMI counts of selected genes (**b**) are shown. **c**, 2D projection of either DR$^+$ (left) or unmodified (right) memory OT-I T cells. **d**, Contribution of DR$^+$ and unmodified memory T cells to the T_{CM} and T_{EM} subsets. **e**, Contribution of DR$^+$ and unmodified OT-I T cells to the 19 MCs that jointly make up the T_{CM} subset. Dots indicate individual mice (n = 3 per condition). Note that all T_{CM} states are generated in near-equal proportions by DR$^+$ and unmodified memory T cells. Depicted scRNAseq data was obtained from 6 individual mice, and was aggregated from 2 independent experiments. *P* values were determined by two-sided Student's T test followed by Bonferroni correction for multiple testing (**d** and **e**). *P* values < 0.05 are indicated.

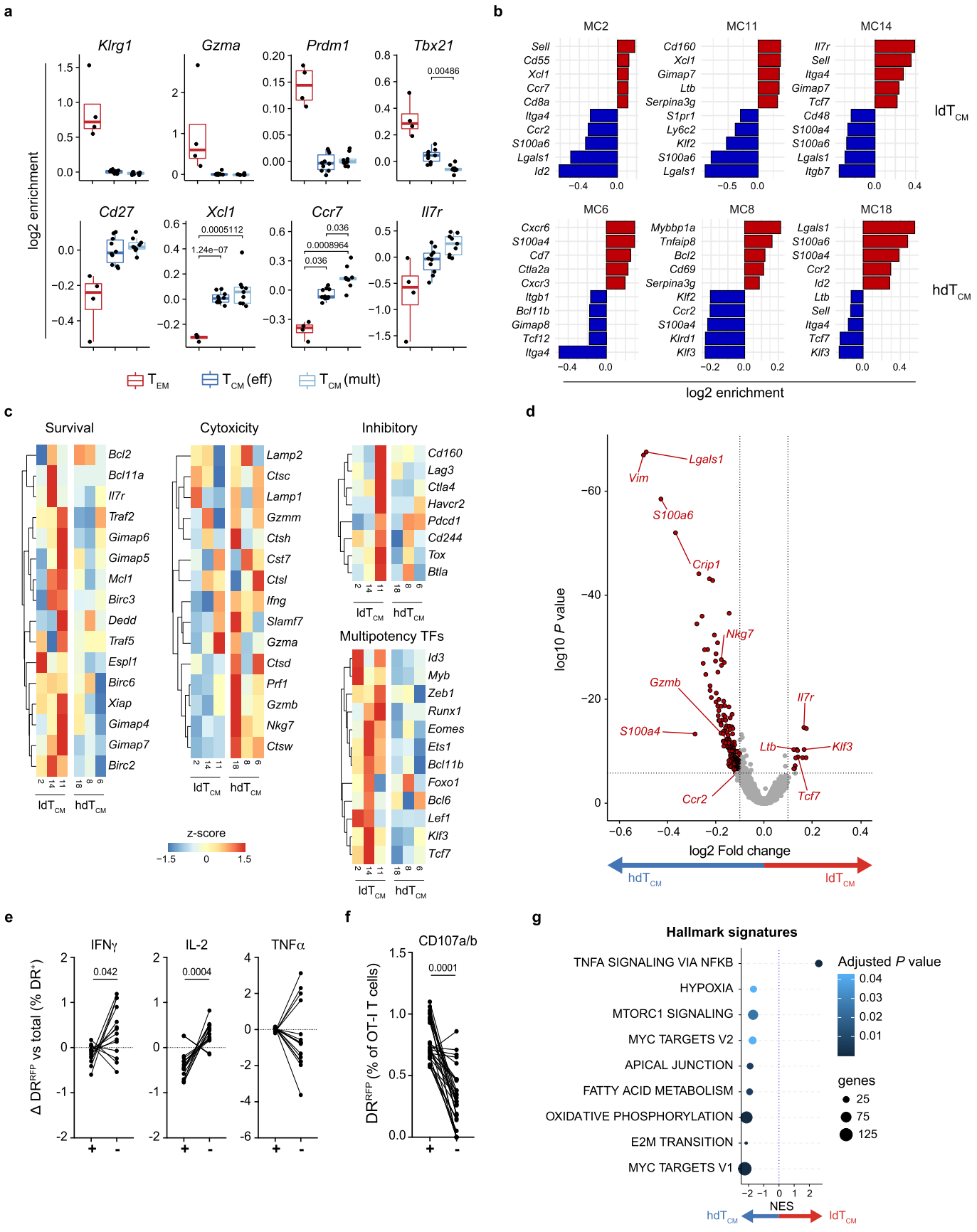

Extended Data Fig. 5 | See next page for caption.

Extended Data Fig. 5 | Replicative history identifies distinct transcriptional states within the T_{CM} pool. Single cell transcriptomic profiling of DR^+ T cells obtained from spleen in memory phase (Day 75 and 85 post *Lm*-OVA infection)**. a**, Log2 enrichment of selected genes in each MC cluster. Boxplots indicate group median and 25^{th}/75^{th} percentiles, whiskers indicate the interquartile range multiplied by 1.5, dots signify individual MCs. The phenotype clusters T_{EM}, T_{CM}(eff.) and T_{CM}(mult.) contain 4, 9 and 10 MCs, respectively. For definition of T_{CM}(eff.) and T_{CM}(mult.), see Fig. 4b. **b**, Top and bottom marker genes of ldT_{CM} (Top, MC2, 11, 14) and hdT_{CM} (Bottom, MC6, 8, 18), see Fig. 4d for ldT_{CM} and hdT_{CM} definitions. **c**, Heatmaps depicting z-score transformed enrichment values of genes related to cell survival (left), cytotoxicity and effector function (middle), inhibitory markers (top-right), and transcription factors involved in T cell multipotency (bottom-right). Expression is depicted for the 3 ldT_{CM} and 3 hdT_{CM} MCs. **d**, Volcano plot depicting differentially expressed genes in ldT_{CM} versus hdT_{CM}. Significantly (adjusted *P* value < 0.05) differentially expressed genes are depicted in red. Selected genes are highlighted. **e**, Cytokine release of $CD27^{HI}KLRG1^{LO}$ DR^+ T cells (isolated from spleen at day >60 post infection) 4 hours post *ex vivo* stimulation. Percentage DR^{RFP} cells within cytokine producers (+) and non-producers (-), relative to the average DR^{RFP} percentage within each sample, is depicted. Lines connect individual *ex vivo* stimulated samples samples (n = 12), obtained from 3 mice. **f**, *Ex vivo* degranulation of $CD27^{HI}KLRG1^{LO}$ DR^+ T cells (isolated from spleen at day >60 post infection) 4 hours post *ex vivo* stimulation. Percentage DR^{RFP} cells within the CD107a/b positive (+) or negative (-) cell populations is depicted. Lines connect individual samples *ex vivo* stimulated samples (n = 17), obtained from 5 mice. **g**, Enrichment of gene signatures from MSigDB (Hallmark) by gene set enrichment analysis comparing ldT_{CM} and hdT_{CM}. Data depicted was accumulated in two independent experiments (3-4 mice per experiment). *P* values were determined by Tukey's HSD test (**a**), Wilcoxon Rank Sum test with Bonferroni correction (**d**), two-sided Wilcoxon signed-rank test (**e, f**), the FGSEA algorithm followed by the Benjamini-Hochberg procedure (**g**). *P* values < 0.05 are indicated.

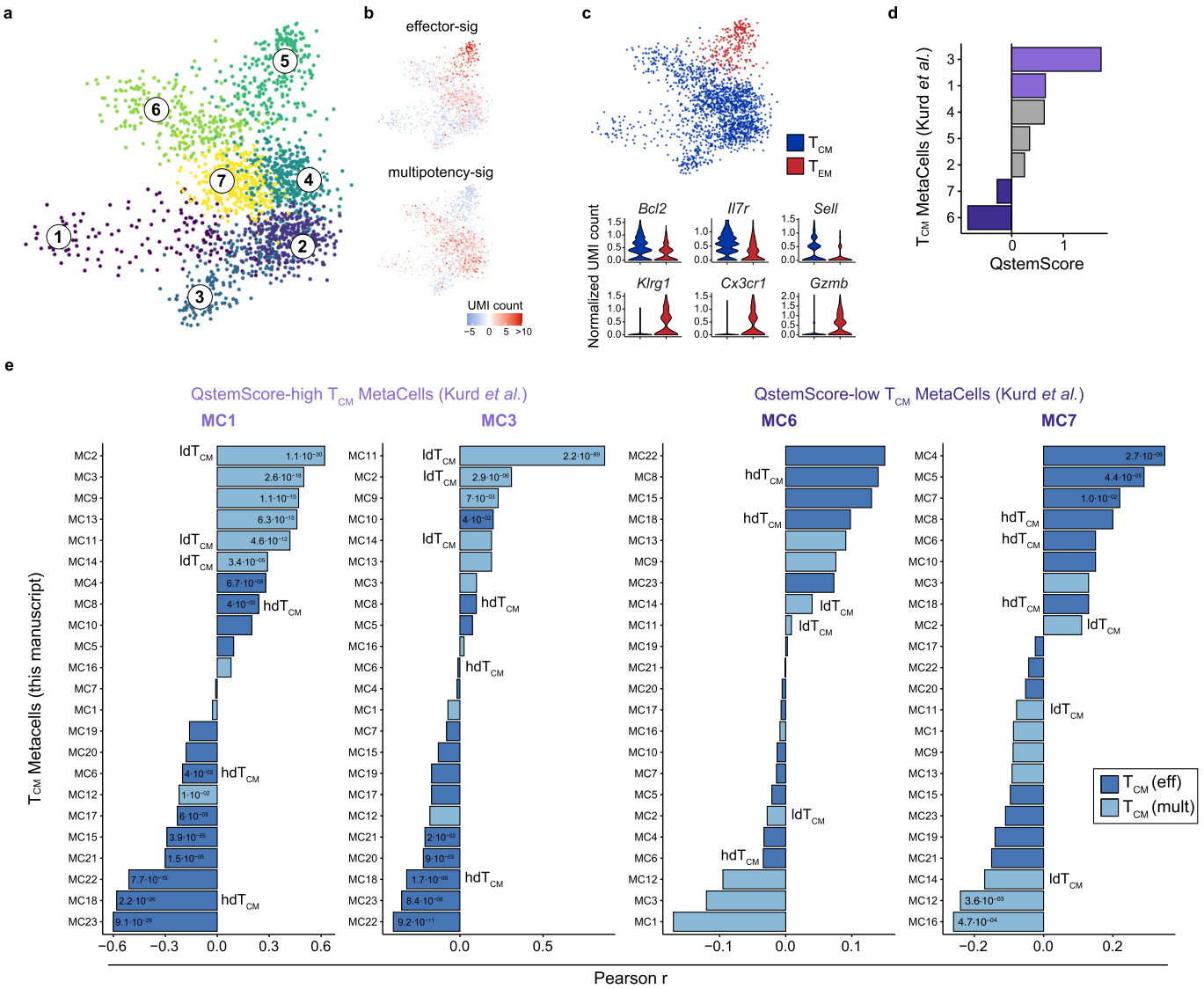

Extended Data Fig. 6 | gp33-specific P14 T_{CM} with increased expression of genes associated with replicative quiescence resemble OT-I ldT_{CM}. Re-analysis of scRNAseq profiled splenic of P14 memory T cells, published in Kurd *et al.* (*Kurd et al., Science Immunology, 2020*). **a-b**, 2D projection of P14 memory T cells 90 days post LCMV infection, colors indicate individual MCs (**a**), or the relative expression of effector- and multipotency-associated genes (**b**). Gene list in Supplementary Table 1. **c**, P14 memory T cells cluster into T_{CM} (blue) and T_{EM} (red). 2D projection colored by subset (top), and violin plots depicting normalized UMI counts of selected genes (bottom) are shown. **d**, QstemScore of all T_{CM} MCs in the Kurd *et al.* dataset. **e**, Pearson correlations between the Kurd et al. P14 T_{CM} MCs that score high (MC1, 3) or low (MC6, 7) for QstemScore, and all OT-I T_{CM} MCs described here. Data are depicted as waterfall plots, asterisks indicate significant correlations. T_{CM}(eff.), T_{CM}(mult.), ldT_{CM} and hdT_{CM} MCs are defined in Fig. 4. *P* values were determined by two-sided Pearson correlation test followed by Bonferroni correction (**e**). *P* values < 0.05 are indicated in the plots.

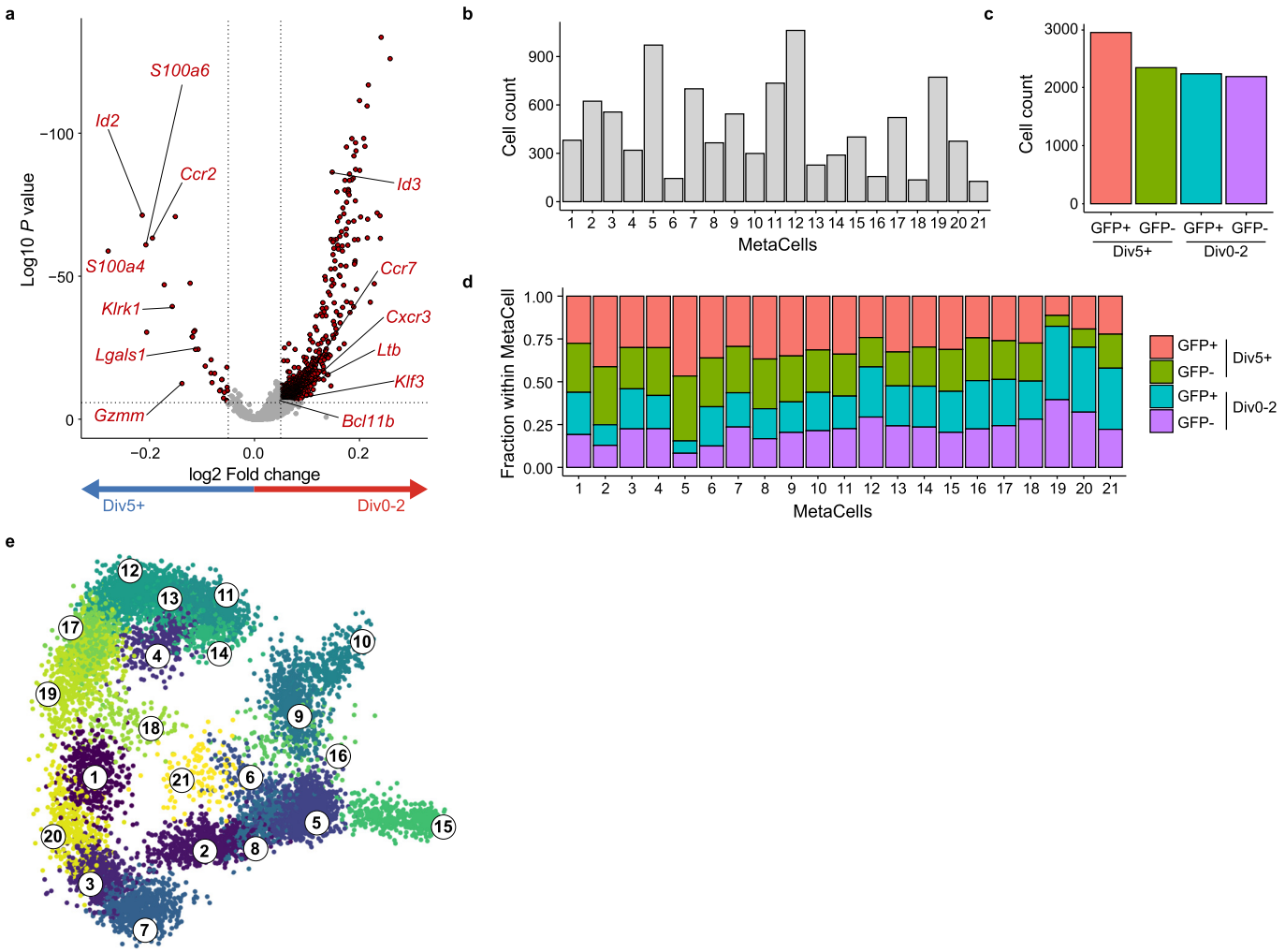

Extended Data Fig. 7 | Single cell mRNA sequencing analysis of highly divided and less divided splenic T_{CM}. a, Volcano plot depicting differentially expressed genes in Div0-2 versus Div5+ T_{CM}. Significantly differentially expressed genes (Adjusted $P < 0.05$) are depicted in red. Selected immune-related genes are highlighted. **b**, Cell count per MC. **c**, Number of sequenced cells per sample included in the analysis. **d**, Sample composition of each MC. **e**, 2D projection, colors indicate different MCs.Depicted scRNAseq data was collected from 4 individual mice. *P* values were determined by Wilcoxon Rank Sum test with Bonferroni correction (**a**).

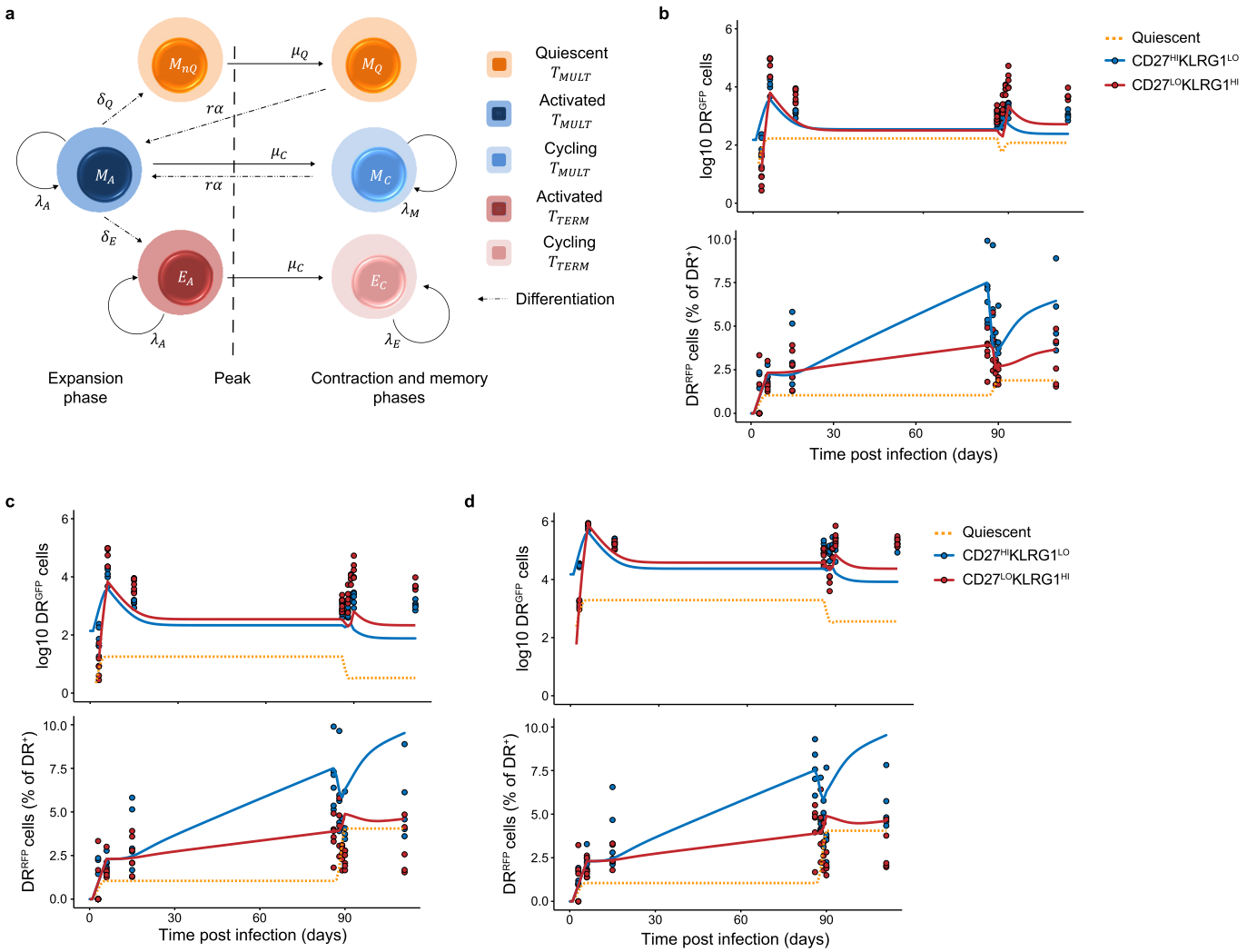

Extended Data Fig. 8 | Modelled T cell responses are consistent with the presence of a replication-competent quiescent T_{CM} population. a, Cartoon of the phenotype model depicting phenotypes, the considered interactions among them and the parameters associated with the interactions. Arrows indicate various events occurring during the response, such as cell division (denoted with λ), differentiation to a different phenotype (denoted with δ), cell death during contraction (denoted with μ), and recruitment toward the secondary response during recall infection (denoted with *r*). Subscripts indicate the phenotype of the cell that the parameter is affecting. Full list of parameters can be found in Supplementary Note 5. **b-d**, Best fit of the modelled T cell response to the experimental measurements depicting either cell numbers (top plot in each panel), or DR^{RFP} percentages (bottom plot in each panel). The total number of quiescent T cells generated was either capped at 1% (**b**) or 0.1% (**c, d**) of the T_{EFF} pool. Lines depict the modeled populations; Dots indicate the experimental measurements obtained from peripheral blood (**b, d**) or spleen (**c**). See Supplementary Note 5 for more details and calculations. Experimental data points are representative of at least two independent experiments, dots indicate individual mice (n = 6 mice per time point).

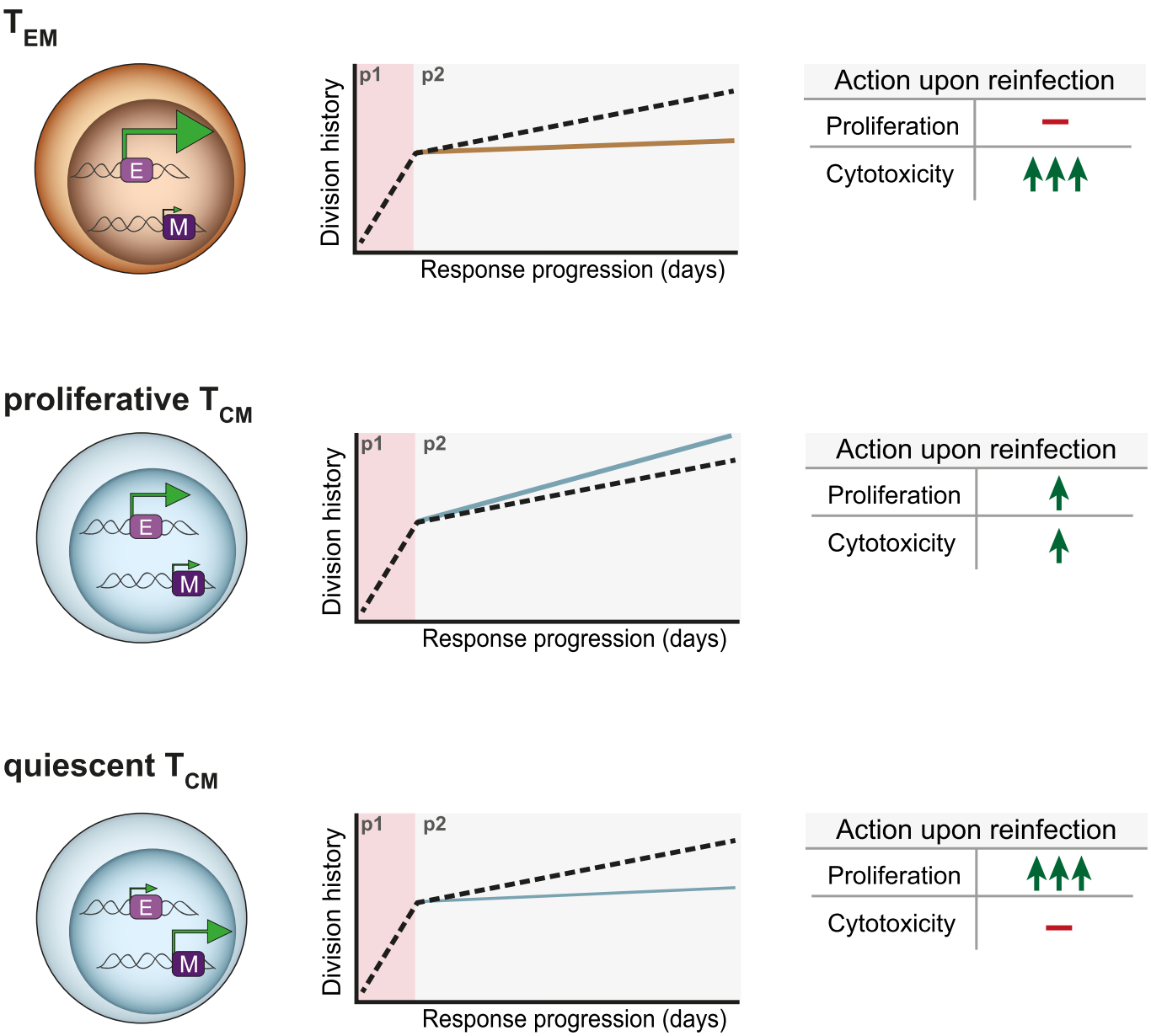

Extended Data Fig. 9 | Model describing replicative behaviors in the CD8⁺ memory T cell pool. Upon infection, antigen-specific CD8⁺ T cells activate and rapidly expand (phase 1, p1). Following pathogen clearance (p2), a subset of memory T cells continues to divide, resulting in a progressive increase in the replicative history of the overall T cell memory pool (dotted line). Within this population, three separate behaviors of transcriptionally disparate memory T cell pools can be distinguished. **Top**) Terminally differentiated T_{EM} cells that cease division after the inflammation phase (p1) and that are marked by high transcription of effector- and minimal expression of multipotency-associated genes ([E], [M]). Upon reactivation, these cells exert rapid effector functions, but lack the potential to re-expand. **Middle**) A subgroup of T_{CM} that continues to proliferate in the memory phase, exhibits diminished levels of multipotency-associated transcripts, and that abundantly expresses effector-associated genes. Although the functionality of these cells upon reinfection requires further study, their heightened expression of effector-associated genes suggests that these cells exert cytotoxic activity upon reinfection. The contribution of these cells to the secondary T_{EFF} pool is limited. **Bottom**) A subgroup of T_{CM} cells that shows low expression of effector-associated genes but increased expression of multipotency-associated genes, and that exists in a near-quiescent state after the inflammation phase. Upon renewed infection, this cell pool is primarily responsible for the generation of a new wave of secondary T_{EFF}. Based on their transcriptional profile, these cells are expected to have limited immediate cytotoxic functions.

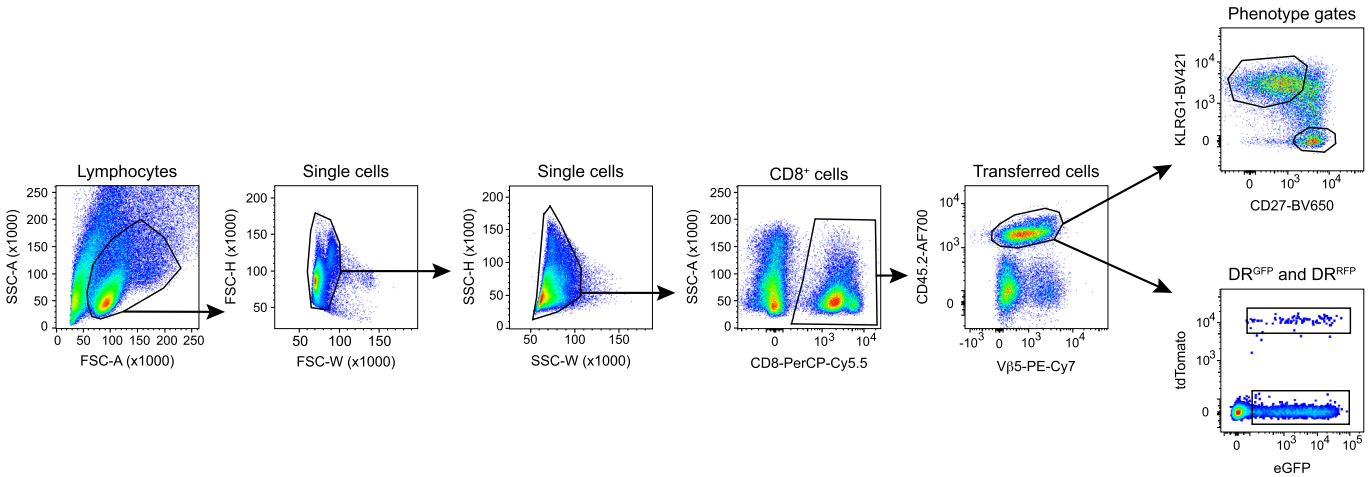

Extended Data Fig. 10 | Gating strategy. General gating applied to flow cytometry data presented in the study. Single lymphocytes were first selected using morphology gates, and were subsequently gated on CD8⁺ T cells and transferred OT-I T cells (Vβ5⁺CD45.2⁺). Next, DR^{RFP} and DR^{GFP} could be directly selected, or first separated by phenotype depending on the analysis. The data presented here was analyzed from blood of a recipient of DR⁺ cells, and was acquired 6 days post infection with *Lm*-OVA. Phenotype gates other than those shown here are defined in their respective figures.

Corresponding author(s): Ton N. Schumacher (t.schumacher@nki.nl) and Ferenc A. Scheeren (f.a.scheeren@lumc.nl)

Last updated by author(s): Feb 14, 2022

Reporting Summary

Nature Research wishes to improve the reproducibility of the work that we publish. This form provides structure for consistency and transparency in reporting. For further information on Nature Research policies, see Authors & Referees and the Editorial Policy Checklist.

Statistics

For all statistical analyses, confirm that the following items are present in the figure legend, table legend, main text, or Methods section.

n/a	Confirmed	
☐	☒	The exact sample size (*n*) for each experimental group/condition, given as a discrete number and unit of measurement
☐	☒	A statement on whether measurements were taken from distinct samples or whether the same sample was measured repeatedly
☐	☒	The statistical test(s) used AND whether they are one- or two-sided *Only common tests should be described solely by name; describe more complex techniques in the Methods section.*
☒	☐	A description of all covariates tested
☒	☐	A description of any assumptions or corrections, such as tests of normality and adjustment for multiple comparisons
☐	☒	A full description of the statistical parameters including central tendency (e.g. means) or other basic estimates (e.g. regression coefficient) AND variation (e.g. standard deviation) or associated estimates of uncertainty (e.g. confidence intervals)
☐	☒	For null hypothesis testing, the test statistic (e.g. *F*, *t*, *r*) with confidence intervals, effect sizes, degrees of freedom and *P* value noted *Give P values as exact values whenever suitable.*
☒	☐	For Bayesian analysis, information on the choice of priors and Markov chain Monte Carlo settings
☒	☐	For hierarchical and complex designs, identification of the appropriate level for tests and full reporting of outcomes
☐	☒	Estimates of effect sizes (e.g. Cohen's *d*, Pearson's *r*), indicating how they were calculated

Our web collection on statistics for biologists contains articles on many of the points above.

Software and code

Policy information about availability of computer code

Data collection	Flow cytometric data was acquired using BDFACSDiva (v8.0) software
Data analysis	Flow cytometric data was analyzed using Flowjo (v10.4.2), R(v6.3.1), FLowCore (v1.52.1). Single cell RNA sequencing data was analyzed using R (v 6.3.1), Seurat (v3.1.1), MetaCell (v0.3.41). Data was visualized using Graphpad (V8.4.1, Prism software) and GGplot(v3.2.1). All analysis codes are available from GitHub (https://github.com/kasbress/DivisionRecorder_analysis).

For manuscripts utilizing custom algorithms or software that are central to the research but not yet described in published literature, software must be made available to editors/reviewers. We strongly encourage code deposition in a community repository (e.g. GitHub). See the Nature Research guidelines for submitting code & software for further information.

Data

Policy information about availability of data

All manuscripts must include a data availability statement. This statement should provide the following information, where applicable:

- Accession codes, unique identifiers, or web links for publicly available datasets
- A list of figures that have associated raw data
- A description of any restrictions on data availability

Transcriptomic data presented in the manuscript have been deposited to the Gene Expression Omnibus, and can be accessed under the GEO accessions GSE169154 and GSE184947. The gp33-specific P14 T cell scRNAseq dataset was retrieved from GEO (accession GSE131847, sample GSM3822202). All statistical source data of the figures presented in the present study are provided with this paper. Indicated gene sets used in gene set enrichment analyses were retrieved from the Molecular Signatures Database (MSigDB) at http://www.gsea-msigdb.org/gsea/msigdb. Any additional data supporting the findings of this study are available from the corresponding author upon request.

Field-specific reporting

Please select the one below that is the best fit for your research. If you are not sure, read the appropriate sections before making your selection.

☒ Life sciences ☐ Behavioural & social sciences ☐ Ecological, evolutionary & environmental sciences

For a reference copy of the document with all sections, see nature.com/documents/nr-reporting-summary-flat.pdf

Life sciences study design

All studies must disclose on these points even when the disclosure is negative.

Sample size	No statistical methods were used to pre-determine sample sizes but our sample sizes are similar to those reported in previous publications (Kok, L. et al. J. Exp. Med. 2020 and Gerlach, C. et al. Science 2013).
Data exclusions	No samples were excluded from analysis
Replication	All findings were replicated in two or three separate experiments, with the exception of the single cell RNA sequencing experiment, in which data was aggregated from multiple separate biological controls (as indicated in the figure legends and methods sections). Al separate experiments yielded comparable results.
Randomization	For the majority of experiments, comparison was done between populations within the same mouse, for which randomization is not required. For experiments where tissues of mice that were sacrificed on different days were compared, mice were stratified according to age and sex. For experiments not involving mouse tissues randomization was not required.
Blinding	No blinding was performed during mouse experiments, since all mice within an experiment received identical treatments. For in vitro experiments, researchers were blinded for sample identity during sample processing and acquisition of data.

Reporting for specific materials, systems and methods

We require information from authors about some types of materials, experimental systems and methods used in many studies. Here, indicate whether each material, system or method listed is relevant to your study. If you are not sure if a list item applies to your research, read the appropriate section before selecting a response.

Materials & experimental systems

n/a	Involved in the study
☐	☒ Antibodies
☐	☒ Eukaryotic cell lines
☒	☐ Palaeontology
☐	☒ Animals and other organisms
☒	☐ Human research participants
☒	☐ Clinical data

Methods

n/a	Involved in the study
☒	☐ ChIP-seq
☐	☒ Flow cytometry
☒	☐ MRI-based neuroimaging

Antibodies

Antibodies used

Antibody Clone Company Catalogue number Dillution used
anti-CD8α-PerCP/Cyanine5.5 SK1 BD Biosciences 565310 1:200
anti-TCR Vb5.1 Vb5.2-PE/Cy7 MR9-4 Biolegend 139508 1:200
anti-CD45.2-Alexa Fluor700 104 Biolegend 109822 1:200
anti-CD27-Brilliant Violet 650 LG.3A10 Biolegend 124233 1:200
anti-CD27-Brilliant Violet 421 LG.3A11 Biolegend 124223 1:200
anti-CD27-APC LG.3A11 Biolegend 124212 1:200
anti-KLRG1-Brilliant Violet 421 2F1/KLRG1 Biolegend 138413 1:200
anti-KLRG1-PE 2F1/KLRG1 Biolegend 138408 1:200
anti-CD62L-Brilliant Violet 785 MEL-14 Biolegend 104440 1:200
anti-CX3CR1-APC SA011F11 Biolegend 149008 1:200
anti-CD43-APC/Cy7 1B11 Biolegend 121220 1:200
anti-IL2-Alexa Fluor 647 JES6-5H4 Biolegend 503814 1:200
anti-IFNγ-Brilliant Violet 785 XMG1.2 Biolegend 505837 1:200
anti-TNFα-Brilliant Violet 650 MP6-XT22 Biolegend 506333 1:200
anti-CD107a- Alexa Fluor 647 1D4B Biolegend 121610 1:200
anti-CD107b- Alexa Fluor 647 M3/84 Biolegend 108512 1:200
anti-Ki67-AF647 B56 BD Biosciences 561126 1:50
anti-CD19-biotin 6D5 Biolegend 115504 1:200
anti-CD20-biotin SA275A11 Biolegend 150414 1:200

anti-CD4-biotin GK1.5 Biolegend 100404 1:200

Validation

Antibody Reactivity Application
anti-CD8α-PerCP/Cyanine5.5 Mouse (QC Testing) Flow cytometry (Routinely Tested)
anti-TCR Vb5.1 Vb5.2-PE/Cy7 Mouse Flow cytometry - Quality tested
anti-CD45.2-Alexa Fluor700 Mouse Flow cytometry - Quality tested
anti-CD27-Brilliant Violet 650 Mouse, Rat, Human Flow cytometry - Quality tested
anti-CD27-Brilliant Violet 421 Mouse, Rat, Human Flow cytometry - Quality tested
anti-CD27-APC Mouse, Rat, Human Flow cytometry - Quality tested
anti-KLRG1-Brilliant Violet 421 Mouse, Human Flow cytometry - Quality tested
anti-KLRG1-PE Mouse, Human Flow cytometry - Quality tested
anti-CD62L-Brilliant Violet 785 Mouse Flow cytometry - Quality tested
anti-CX3CR1-APC Mouse Flow cytometry - Quality tested
anti-CD43-APC/Cy7 Mouse Flow cytometry - Quality tested
anti-IL2-Alexa Fluor 647 Mouse Intracellular Staining for Flow Cytometry - Quality tested
anti-IFNγ-Brilliant Violet 785 Mouse Intracellular Staining for Flow Cytometry - Quality tested
anti-TNFα-Brilliant Violet 650 Mouse Intracellular Staining for Flow Cytometry - Quality tested
anti-CD107a- Alexa Fluor 647 Mouse Flow cytometry - Quality tested
anti-CD107b- Alexa Fluor 647 Mouse Flow cytometry - Quality tested; Immunocytochemistry - Verified
anti-Ki67-AF647 Human (QC Testing), Mouse (Tested in Development), Rat, Rhesus (Reported) Intracellular staining (flow cytometry) (Routinely Tested)
anti-CD19-biotin Mouse Flow cytometry - Quality tested
anti-CD20-biotin Mouse Flow cytometry - Quality tested
anti-CD4-biotin Mouse Flow cytometry - Quality tested

Eukaryotic cell lines

Policy information about cell lines

Cell line source(s)

Platinum-E cell line was obtained from Cell Biolabs, Inc and the HEK 293T cell line was originally acquired from ATCC and kept over many passages within the Netherlands Cancer Institute. A mouse embryonic fibroblast (MEF) cell line from the Ai9 mouse strain was generated by modification of E14.5 embryonic fibroblasts with a retroviral vector encoding short-hairpin RNA directed against the p53 mRNA.

Authentication

cell lines used were not authenticated

Mycoplasma contamination

All cell lines have been tested for Mycoplasma contamination and tested negative

Commonly misidentified lines
(See ICLAC register)

HEK 293T is named by ICLAC; usage of this cell line is not dependent on its correct identity, but rather the introduced reporter construct.

Animals and other organisms

Policy information about studies involving animals; ARRIVE guidelines recommended for reporting animal research

Laboratory animals

species: mus musculus,
strains: C57bl/6.Ly5.1, OT-I, Ai9, UCB-GFP
sex: male and female
age: 8-12 weeks

Wild animals

study did not involve wild animals

Field-collected samples

study did not involve samples collected from the field

Ethics oversight

All animal experiments were approved by the Animal Welfare Committee of the NKI, in accordance with national guidelines.

Note that full information on the approval of the study protocol must also be provided in the manuscript.

Flow Cytometry

Plots

Confirm that:

☒ The axis labels state the marker and fluorochrome used (e.g. CD4-FITC).

☒ The axis scales are clearly visible. Include numbers along axes only for bottom left plot of group (a 'group' is an analysis of identical markers).

☒ All plots are contour plots with outliers or pseudocolor plots.

☒ A numerical value for number of cells or percentage (with statistics) is provided.

Methodology

Sample preparation	See method section of manuscript
Instrument	Fortessa, BD Bioscience
Software	Data collection: BDFACSDiva (v8.0) software Data analysis: Flow cytometric data was analysed using Flowjo (v10.4.2), R(v6.3.1), FLowCore (v1.52.1)
Cell population abundance	Populations were sorted at >98% purity, determined by flow cytometric analysis of post-sort samples
Gating strategy	Transferred DivisionRecorder+ cells were identified as CD8a+vb5+CD45.2+GFP+

☒ Tick this box to confirm that a figure exemplifying the gating strategy is provided in the Supplementary Information.